A non-Hermitian $\mathcal{PT}-$symmetric Bose-Hubbard model: eigenvalue rings from unfolding higher-order exceptional points

E. M. Graefe[a]**, U. Günther**[b]**, H. J. Korsch**[a]**, A. E. Niederle**[a]

[a] Technical University Kaiserslautern,
D-67663 Kaiserslautern, Germany
[b] Research Center Dresden-Rossendorf, POB 510119,
D-01314 Dresden, Germany

E-mail: `graefe@physik.uni-kl.de`, `u.guenther@fzd.de`,
`korsch@physik.uni-kl.de`, `a.niederle@gmx.de`

Abstract. We study a non-Hermitian $\mathcal{PT}-$symmetric generalization of an N-particle, two-mode Bose-Hubbard system, modeling for example a Bose-Einstein condensate in a double well potential coupled to a continuum via a sink in one of the wells and a source in the other. The effect of the interplay between the particle interaction and the non-Hermiticity on characteristic features of the spectrum is analyzed drawing special attention to the occurrence and unfolding of exceptional points (EPs). We find that for vanishing particle interaction there are only two EPs of order $N + 1$ which under perturbation unfold either into $[(N + 1)/2]$ eigenvalue pairs (and in case of $N + 1$ odd, into an additional zero-eigenvalue) or into eigenvalue triplets (third-order eigenvalue rings) and $(N + 1) \bmod 3$ single eigenvalues, depending on the direction of the perturbation in parameter space. This behavior is described analytically using perturbational techniques. More general EP unfoldings into eigenvalue rings up to $(N + 1)$th order are indicated.

1. Introduction

Physical models usually describe only a rather small separated system uncoupled from the rest of the world. In quantum physics the behavior of such a system is governed by a Hermitian Hamiltonian operator. If one wants to take the coupling to some external world into account, one ends up with the description of an open quantum system. A somehow crude but instructive way to describe such open quantum systems is the use of effective non-Hermitian Hamiltonians. These descriptions in general yield complex eigenvalues whose imaginary parts describe the rates with which an eigenstate decays to the external world. Most often non-Hermitian Hamiltonians are introduced heuristically, although this approximative description can be achieved in a mathematically satisfactory way for example by applying the Feshbach projection operator technique [1].

Thinking of the description of open quantum systems it might be surprising that there is a whole class of non-Hermitian Hamiltonians which in some parameter

regions give rise to purely real eigenvalues and to unitary dynamics. These so-called $PT−$symmetric Hamiltonians [2–7] possess space-time-reflection symmetry, e.g., they commute with the PT operator, where the operators P and T are defined by their effects on the position and momentum operator x and p as

$$
\begin{aligned}
P: & \quad x \mapsto -x, \quad p \mapsto -p \\
T: & \quad x \mapsto x, \quad p \mapsto -p, \quad \mathrm{i} \mapsto -\mathrm{i}.
\end{aligned} \tag{1}
$$

In some parameter region, the region of unbroken $PT−$symmetry, all eigenvalues of $PT−$symmetric Hamiltonians are purely real and the behavior of the system is similar to that of Hermitian quantum systems. To get a feeling for the underlying reasons of this "pseudo-closed" behavior of an open system, one can think of it in terms of a balanced probability-flow [8]. Replacing the condition of Hermiticity by the condition of $PT−$symmetry therefore yields as well a fully consistent quantum theory, which attracted a lot attention in the last years and actually stimulated the research in other fields of physics like complexified classical systems, supersymmetry and quantum field theory [9].

At first glance one might get the impression that the non-Hermiticity is nothing but a small perturbation which does not change the behavior of a system too much compared to the Hermitian case, despite an additional decay behavior, or it may even be equivalent to a Hermitian theory in the presence of $PT−$symmetry. But actually non-Hermitian physics can differ radically from Hermitian physics, especially in the presence of eigenvalue degeneracies. While a Hermitian operator is always diagonalizable (eigenvalues may coalesce, nevertheless they always correspond to distinct eigenvectors), for a non-Hermitian Hamiltonian the occurrence of nontrivial Jordan blocks in its spectral decomposition is possible – there may be points in parameter space at which both eigenvalues *and* eigenvectors coalesce, so-called exceptional points (EPs) [10, 11]. The occurrence of EPs in a system has drastic effects on the systems behavior, especially concerning adiabatic features and geometric phases. For the occurrence of EPs in various physical models see, for example and not aiming at any completeness [1, 12–28]. In the theory of $PT−$symmetric quantum systems EPs naturally occur as phase-transition points between sectors of exact $PT−$symmetry and sectors of spontaneously broken $PT−$symmetry.

The field of $PT−$symmetric Hamiltonians is still young and the underlying mathematical structures are not completely understood yet. Therefore in the last few years the interest in comparatively simple systems with a finite dimensional Hilbert space, especially $PT−$symmetric matrix Hamiltonians, was rapidly growing [23,24,29]. In this context most investigations focused on the mathematical behavior of simple matrix models, without demanding them to represent a physical system. Nevertheless under special conditions there are a lot of physical systems which indeed justify the description via a finite matrix model. In the present paper we introduce a $PT−$symmetric generalization of a prominent Hermitian matrix model, a two-mode Bose-Hubbard Hamiltonian, which in the case of N particles acts on an $N + 1$ dimensional Hilbert space.

The Bose-Hubbard Hamiltonian is a simple description of interacting bosons on a lattice, which only takes one state per lattice site into account. Originally the Hubbard model is a basic model of solid state physics, where it is mostly addressed in its fermionic version to describe the behavior of electrons in solids. In the last few years it is enjoying a renaissance in the context of Bose-Einstein condensates (BEC) in optical potentials. Due to the extremely low temperatures and the precise periodicity

of the optical potential these systems provide the possibility of a clean experimental realization of many kinds of theoretical models for interacting many-particle systems. One prominent example is the superfluid to Mott insulator phase transition which was realized in a BEC in a three-dimensional optical potential [30].

Investigating large M-mode, N-particle Bose-Hubbard systems quickly goes beyond the scope of numerical manageability. Therefore, due to its simple structure, the two-mode case, which one may think of describing a BEC in a double well trap, became a standard model [31–36]. In the present paper we introduce an effective non-Hermiticity to this two-mode Bose-Hubbard Hamiltonian in a $\mathcal{PT}-$symmetric way, which one can imagine as an additional source and sink of equal strength. A closely related – and slightly more physical – model would include only a sink and would yield complex eigenvalues with a negative imaginary part, describing a decay of particles. First theoretical results for this non-Hermitian two-mode Bose-Hubbard system were presented in [37]. As a possible realization one can think of a BEC in a double well trap, where the condensate could escape from one of the traps via tunneling. Another possibility would be the outcoupling of atoms from one of the traps via radiofrequency [38].

In the present paper we analyze the spectrum of the $\mathcal{PT}-$symmetric two-mode Bose-Hubbard system where we draw special attention to the occurrence and the unfolding of EPs. Numerical results are presented to illustrate the characteristic behavior of this unfolding. Furthermore we use perturbative methods which allow for analytic descriptions. Basic tools are the Le Verrier-Faddeev method [39] for the derivation of the coefficients of characteristic polynomials of matrices and the Newton-polygon technique for the extraction of the dominant powers of polynomial perturbations [11, 40, 41].

In detail the paper is organized as follows: In section 2 we introduce the two-mode Bose-Hubbard Hamiltonian and its $\mathcal{PT}-$symmetric generalization and review the basic vocabulary according to Hermitian and non-Hermitian degeneracies. We discuss the analytically solvable limit of vanishing interaction in section 3 before we present numerical results on the spectrum for non-vanishing interaction in section 4. Finally, in section 5, we investigate some of the features of the spectrum previously found in the numerical studies analytically using perturbative methods.

2. Bose-Hubbard model and basic non-Hermitian vocabulary

The physical setup under consideration is a BEC in a double well potential which at low temperatures can be analyzed in a two-mode approximation. The corresponding Hamiltonian is that of a second quantized many particle system of Bose-Hubbard type

$$H = \varepsilon \left(a_1^\dagger a_1 - a_2^\dagger a_2 \right) + v \left(a_1^\dagger a_2 + a_2^\dagger a_1 \right) + \frac{c}{2} \left(a_1^\dagger a_1 - a_2^\dagger a_2 \right)^2, \qquad (2)$$

where a_j, $a_j^\dagger$ are bosonic particle annihilation and creation operators for the $j-$th mode, 2ε is the on-site energy difference, v controls the single particle tunneling and c the interaction strength between the particles. In order to simplify the discussion we assume here that both v, and c are positive[1]. The Hamiltonian commutes with the

---

[1]) Note that the energy spectrum stays the same if the sign of v is altered, while it is turned upside down $E_n \rightarrow -E_n$ if the sign of c is altered, which does not change the subsequent discussions in principle. Experimentally both negative and positive values of the interaction are possible and can actually be modulated via a Feshbach resonance [42].

particle number operator

$$N = a_1^\dagger a_1 + a_2^\dagger a_2, \tag{3}$$

so that the total number N of particles is conserved.

It is convenient to introduce angular momentum operators according to the Schwinger representation

$$L_x = \frac{1}{2}\left(a_1^\dagger a_2 + a_2^\dagger a_1\right)$$
$$L_y = \frac{1}{2i}\left(a_1^\dagger a_2 - a_2^\dagger a_1\right) \tag{4}$$
$$L_z = \frac{1}{2}\left(a_1^\dagger a_1 - a_2^\dagger a_2\right),$$

which obey the $su(2)$ commutation relation

$$[L_x, L_y] = iL_z, \tag{5}$$

and its cyclic permutations. In terms of these operators the Hamiltonian (2) assumes the form

$$H = 2\varepsilon L_z + 2v L_x + 2c L_z^2. \tag{6}$$

Thus for $\varepsilon, v, c \in \mathbb{R}$ it is an element of the universal enveloping algebra[2] $\mathcal{U}(su(2))$ of the $su(2)$ Lie algebra in its angular momentum $l = N/2$ representation. In addition we will often use the Lie algebra elements $L_\pm = L_x \pm iL_y$ with commutation relations $[L_z, L_\pm] = \pm L_\pm, \quad [L_-, L_+] = -2L_z$.

In the standard basis of the angular momentum algebra $|l, m\rangle$, which can be defined by the relations

$$L_\pm|l, m\rangle = \sqrt{(l \mp m)(l \pm m + 1)}|l, m \pm 1\rangle, \qquad L_z|l, m\rangle = m|l, m\rangle \tag{7}$$

with $l = N/2$, the Hamiltonian H takes the form of a tridiagonal $(N + 1) \times (N + 1)-$matrix

$$H = \begin{pmatrix} d_l + c_l & v_{l-1} & \cdots & 0 & 0 \\ v_{l-1} & d_{l-1} + c_{l-1} & \cdots & 0 & 0 \\ \vdots & \ddots & \ddots & \vdots & \vdots \\ 0 & 0 & \cdots & -d_{l-1} + c_{l-1} & v_{l-1} \\ 0 & 0 & \cdots & v_{l-1} & -d_l + c_l \end{pmatrix}$$

$$d_m := 2\varepsilon|m|, \qquad c_m := 2cm^2, \quad -l \le m \le l$$
$$v_m := v\sqrt{(l + m + 1)(l - m)} = v_{-(m+1)}. \tag{8}$$

In the following, for the non-Hermitian generalization of the Bose-Hubbard Hamiltonian and the structure analysis of the characteristic polynomials (see equation (44) and below) another representation of the angular momentum basis in terms of monomials in a complex variable will turn out to be most convenient. The representation (7) can be described in a standard way as monomials in a variable $\xi \in \mathbb{C}$ as (see, e.g., [46, 47])

$$|l, m\rangle \cong f_m(\xi) = \frac{\xi^{l+m}}{\sqrt{(l - m)!(l + m)!}} \in \mathcal{H}_l, \qquad -l \le m \le l \tag{9}$$

---

[2]) For universal enveloping algebras see, e.g., [43–45].

with the normalization condition

$$\langle l, j|l, m\rangle = \frac{(2l+1)2l!}{\pi} \int \frac{\overline{f_j(\xi)}f_m(\xi)}{(1+|\xi|^2)^{2l+2}}d^2\xi = \delta_{jm}, \quad d^2\xi := d(\operatorname{Im}\xi)d(\operatorname{Re}\xi). \qquad (10)$$

Here, $\mathcal{H}_l$ denotes the space of polynomials in ξ of degree less or equal $2l+1$ [46, 47], in which the $SU(2)$ group representation acts. In the representation (9) the angular momentum operators act as first-order differential operators

$$L_z = \xi\partial_\xi - l, \qquad L_+ = -\xi^2\partial_\xi + 2l\xi, \qquad L_- = \partial_\xi \qquad (11)$$

and yield again the relations (7).

We note that (7, 9, 10, 11) is the standard complex irreducible representation (irrep) of the real Lie algebra $su(2)$ (and the corresponding compact, simply connected group $SU(2)$) for fixed angular momentum l [46, 47]. The advantage of this complex $(2l+1)-$dimensional irrep is its straightforward linear extendability to the complexification of $su(2)$, i.e., to $sl(2, \mathbb{C})$ (see proposition 4.6 in [48]). Such a complexification is necessarily encountered when one passes from real coefficients ε, v, g in the Hamiltonian (2) to complex ones — as in our case when we pass from the Hermitian H to the non-Hermitian $\mathcal{PT}-$symmetric H by assuming ε to be purely imaginary. Under the specific embedding $su(2) \hookrightarrow sl(2, \mathbb{C})$ the irrep dimension $2l+1$ remains fixed. For completeness, we further note that the complexification of the non-compact, not simply connected real $SU(1,1)$ yields another embedding $su(1,1) \hookrightarrow sl(2, \mathbb{C})$ with corresponding extensions of the infinite dimensional $su(1,1)$ irreps [47, 48]. Below we will consider boosts within the $(2l+1)-$dimensional irrep of the $su(2) \hookrightarrow sl(2, \mathbb{C})$ embedding, not involving infinite dimensional $su(1,1)-$related irreps (and corresponding matrices of countably infinite order), i.e. we keep within the $su(2) \hookrightarrow sl(2, \mathbb{C})$ induced irrep although boosts are naturally connected with $SU(1,1)$ transformations.

The previous considerations justify the expansion of a non-Hermitian generalization of the Hamiltonian (2) in the same basis (7) which yields a non-Hermitian matrix representation as a generalization of the matrix (8).

In the present paper we investigate a situation, where we assume the on-site energy difference ε of the two-mode Bose-Hubbard model (2) to be complex, while the parameters c and v are kept real. In particular, we focus on the case of a BEC in a symmetric double well, where the real parts of the energies of both modes are equal and therefore ε is purely imaginary $\varepsilon \equiv -i\gamma,\ \gamma \in \mathbb{R}$

$$H = -2i\gamma L_z + 2vL_x + 2cL_z^2. \qquad (12)$$

Physically such an imaginary on-site energy difference can be achieved by coupling the modes to a continuum so that they will be unstable — decaying and amplifying in a balanced way. Although $\varepsilon \in i\mathbb{R}$ spoils the Hermiticity of the Hamiltonian H in a usual Euclidian Hilbert space, it nevertheless leaves H Hermitian in a Hilbert space with an indefinite inner product structure, i.e., in a so-called Krein space [49–56]. This is easily seen from the explicit matrix structure, which is essentially equivalent to (8) with the substitution $\varepsilon \equiv -i\gamma$. The matrix H is not only symmetric, $H = H^T$, rather it holds also

$$H = \mathcal{P}H^\dagger\mathcal{P} \qquad (13)$$

where $\mathcal{P}$ is the standard involutory permutation (sip) matrix

$$\mathcal{P} = \begin{pmatrix} 0 & 0 & \cdots & 0 & 1 \\ 0 & 0 & \cdots & 1 & 0 \\ \vdots & \vdots & \ddots & \vdots & \vdots \\ 0 & 1 & \cdots & 0 & 0 \\ 1 & 0 & \cdots & 0 & 0 \end{pmatrix}, \qquad \mathcal{P}^2 = I \tag{14}$$

which is similar to an indefinite diagonal matrix

$$\mathbb{R}^{2n\times 2n} \ni \mathcal{P} \sim \begin{pmatrix} I_n & 0 \\ 0 & -I_n \end{pmatrix}, \qquad \mathbb{R}^{(2n+1)\times(2n+1)} \ni \mathcal{P} \sim \begin{pmatrix} I_{n+1} & 0 \\ 0 & -I_n \end{pmatrix}. \tag{15}$$

Obviously, $\mathcal{P}$ can be interpreted as parity operator which interchanges the $a_1^\dagger a_1-$ and $a_2^\dagger a_2-$related modes in (2) as

$$\mathcal{P}: \quad |l,m\rangle \ \mapsto \ \mathcal{P}|l,m\rangle = |l,-m\rangle. \tag{16}$$

Denoting, as usual, the involution operator of the complex conjugation – the time reversal operator of quantum mechanics – by $\mathcal{T}$, where $\mathcal{T}^2 = I$, and taking into account that

$$H^\dagger = \mathcal{T}H^T\mathcal{T} = \mathcal{T}H\mathcal{T} \tag{17}$$

we find that the Hamiltonian H for $\varepsilon \in i\mathbb{R}$ is $\mathcal{PT}-$symmetric

$$[\mathcal{PT}, H] = 0. \tag{18}$$

According to (13) it is self-adjoint in the Krein space $\mathcal{K}_\mathcal{P}$ with the indefinite inner product $[.,.]_\mathcal{P} = \langle .|\mathcal{P}|.\rangle$. Therefore the spectrum of H will contain not only real branches, but also pairwise complex conjugate branches and exceptional points (branch points) at the transitions between real and complex sectors of the spectrum. This is the typical behavior of a $\mathcal{PT}-$symmetric operator. For completeness, we note that purely real branches correspond to parameter regions of exact $\mathcal{PT}-$symmetry (H and its eigenfunctions are $\mathcal{PT}-$symmetric), whereas pairwise complex conjugate eigenvalues correspond to regions of spontaneously broken $\mathcal{PT}-$symmetry (in contrast to H its eigenfunctions are not $\mathcal{PT}-$symmetric).

In the more general case of complex on-site energy difference $\varepsilon \in \mathbb{C}$ where neither real nor imaginary part are vanishing, the $\mathcal{PT}-$symmetry of the system is spoilt and one obtains, in general, a spectrum not containing regions of purely real eigenvalues.

For a Hermitian operator the spectrum is purely real. Possible level crossing (degeneration) points will be so-called diabolical points (DPs) [57], which are connected with diagonalizable spectral decomposition, where algebraic multiplicity n_a and geometric multiplicity n_g [11] of the degenerate eigenvalues λ coincide[3], $n_a(\lambda) = n_g(\lambda)$ and one finds a symmetry enhancement[4]. In addition to these diabolic degeneration points, for a non-Hermitian operator the occurrence of exceptional points (EPs) is possible and even generic. EPs are parameter configurations at which for a corresponding degenerate eigenvalue λ the algebraic multiplicity $n_a(\lambda)$ is exceeding the geometric multiplicity, $n_g(\lambda) < n_a(\lambda)$. This is connected with a non-diagonalizable spectral decomposition of the operator (matrix) [10, 11], i.e., the formation of non-trivial Jordan-block structures [39, 59] and Jordan chains of algebraic eigenvectors

---

[3]) Eigenvalues of diagonalizable matrices are called semi-simple (see e.g. [58]) and in case of $n_g(\lambda) = n_a(\lambda) = 1$ simple.

[4]) For a $k-$fold DP a $U(k)$ rotation symmetry occurs within the span of the degenerate eigenvectors.

(associated vectors). Subsequently, we use the term mth-order EP for an EP which is associated with an mth-order Jordan block in the spectral decomposition.

The EPs and DPs live on certain hypersurfaces $\mathcal{V}_j$ in the underlying parameter space $\mathcal{M} \supset \mathcal{V}_j$ of the model. They are, in general, of various co-dimensions and form a so-called stratified manifold $\mathcal{V} = \bigcup_j \mathcal{V}_j$ (see, e.g., [60]). Depending on a concrete parameter perturbation the system may move along the stratified manifold $\mathcal{V}$ passing from one degeneration type to another one, or, more generically, it may escape from $\mathcal{V}$ so that the degeneration disappears and an EP or DP unfolds into non-degenerate eigenvalues.

In the following sections we will analyze the occurrence and the unfolding of EPs for our Bose-Hubbard model. We will find that in the limit of vanishing particle interaction the model can be solved analytically and that there exist only two EPs of order $N + 1$. In dependence on the direction of the perturbation in parameter space each of these EPs unfolds either into $[(N + 1)/2]$ eigenvalue pairs[5] (and, in case of $N + 1$ odd, into an additional zero-eigenvalue) or into eigenvalue triplets (third-order eigenvalue rings) and $(N + 1) \bmod 3$ single eigenvalues.

3. The limit of vanishing interaction

For vanishing interaction, $c = 0$, the Hamiltonian H in (12) is a complex linear combination of $su(2)$ Lie algebra elements

$$H = 2(-i\gamma L_z + vL_x) \in sl(2, \mathbb{C}). \tag{19}$$

Figure 1 shows real and imaginary parts of the eigenvalues of H as a function of γ for an example with $N = 11$ particles and fixed $v = 1$. All eigenvalues are purely real for $|\gamma| < 1$ and purely imaginary for $|\gamma| > 1$. For $|\gamma| = 1$ we observe a degeneracy of all eigenvalues, which will turn out to correspond to a full Jordan block, resp. an EP of order N+1. Furthermore the real and imaginary parts are axis symmetric with regard to both axes $E_n = 0$ and $\Gamma_n = 0$ — a behavior which is due to the high symmetry of the Hamiltonian (19). The eigenvalues can be easily obtained analytically by diagonalizing H in case of $|\gamma| \neq |v|$ and bringing it to its non-trivial Jordan block form in case of $|\gamma| = |v|$.

For this purpose we make use of the Baker-Campbell-Hausdorff formula and the $su(2)$ commutation relations (5) to obtain the well known rotations and boosts over the algebra $su(2)$ specifically needed for our analysis

$$e^{-i\theta L_y} L_z e^{i\theta L_y} = \cos(\theta)L_z + \sin(\theta)L_x, \tag{20}$$

$$e^{\alpha L_y} L_z e^{-\alpha L_y} = \cosh(\alpha)L_z + i\sinh(\alpha)L_x, \tag{21}$$

$$e^{-i\theta L_x} L_y e^{i\theta L_x} = \cos(\theta)L_y + \sin(\theta)L_z. \tag{22}$$

With the help of the boost (21) and the identification

$$\cosh(\alpha) = \frac{\gamma}{\sqrt{\gamma^2 - v^2}}, \qquad \sinh(\alpha) = \frac{v}{\sqrt{\gamma^2 - v^2}} \tag{23}$$

the Hamiltonian (19) can be reshaped as

$$\begin{aligned} H &= -2i\sqrt{\gamma^2 - v^2} \left[\cosh(\alpha)L_z + i\sinh(\alpha)L_x\right] \\ &= -2\sqrt{v^2 - \gamma^2} e^{\alpha L_y} L_z e^{-\alpha L_y}. \end{aligned} \tag{24}$$

---

[5]) The notation $[a]$ stands for the floor function which yields the highest integer less or equal $a \in \mathbb{R}$.
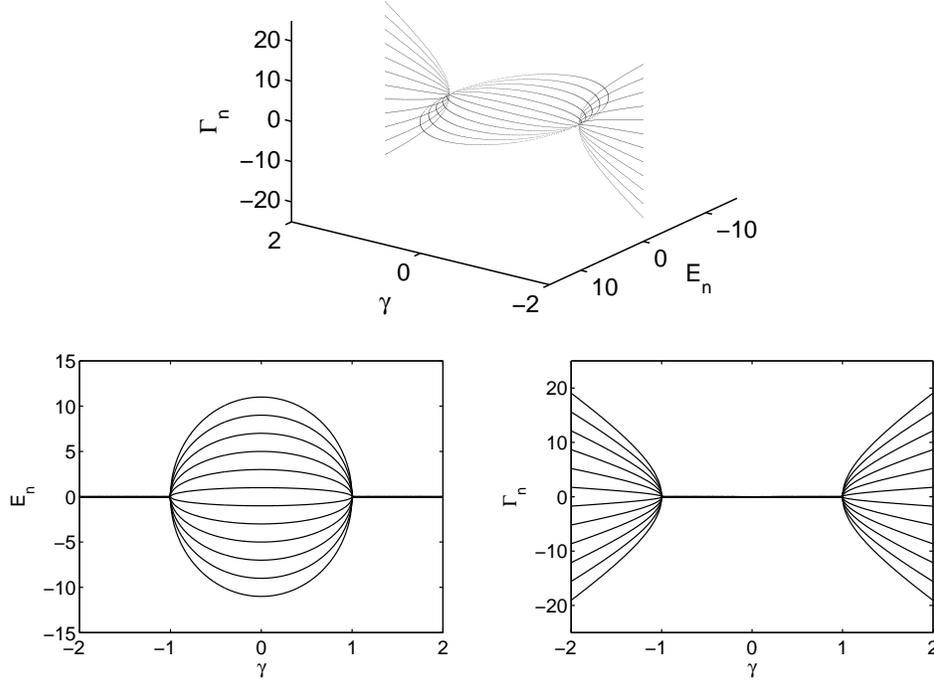
Figure 1. Real- and imaginary parts of the eigenvalues $\lambda_n = E_n - i\Gamma_n$ of the Bose-Hubbard Hamiltonian (19) as a function of the non-Hermiticity γ for $v = 1$ and $N = 11$ particles for vanishing interaction $c = 0$.

From the fact that the irrep (9) remains valid for any complex extension of $su(2)$ it follows the completeness of the basis vectors

$$I = \sum_{m=-l}^{l} |l,m\rangle\langle l,m| \tag{25}$$

and with it

$$\langle l,j|H|l,k\rangle = -2\sqrt{v^2 - \gamma^2}\sum_{m,m'=-l}^{l} \langle l,j|e^{\alpha L_y}|l,m\rangle\langle l,m|L_z|l,m'\rangle\langle l,m'|e^{-\alpha L_y}|l,k\rangle$$

$$= -2\sqrt{v^2 - \gamma^2}\sum_{m=-l}^{l} S_{jm}^{-1}mS_{mk} \tag{26}$$

where

$$S_{mk} := \langle l,m|e^{-\alpha L_y}|l,k\rangle. \tag{27}$$

For $|\gamma| \neq |v|$ the boost functions (23) remain finite so that $|\alpha| < \infty$ and S remains regular. Therefore, S acts as similarity transformation which diagonalizes the Hamiltonian (19). The eigenvalues of H can be read off from (26) as

$$\lambda_n = E_n - i\Gamma_n = n\sqrt{v^2 - \gamma^2} \tag{28}$$

where $n = -N, -N+2, \ldots, N-2, N$. In the limit $\gamma \to \pm v$ the diagonalization breaks down and the boost becomes singular: $|\alpha| \to \infty$. Instead of eq. (21) we may use a rotation (22) with $\theta = -\pi/2$, i.e.

$$e^{i\pi L_x/2} L_y e^{-i\pi L_x/2} = -L_z \,. \tag{29}$$

This allows us to represent the Hamiltonian as

$$H = 2v(\mp iL_z + L_x) = 2ve^{i\pi L_x/2}(\pm iL_y + L_x)e^{-i\pi L_x/2}$$
$$= 2ve^{i\pi L_x/2}L_\pm e^{-i\pi L_x/2}, \tag{30}$$

so that with $R_{nk} := \langle l, n|e^{-i\pi L_x/2}|l, k\rangle$ we have

$$\langle l, j|H|l, k\rangle = 2vR_{jm}^{-1}\langle l, m|L_\pm|l, n\rangle R_{nk}, \qquad \det(R) \neq 0. \tag{31}$$

According to (7) only the elements $\langle l, k\pm1|L_\pm|l, k\rangle$ are non-vanishing. This means that the matrix $\langle l, m|L_\pm|l, n\rangle$ is subdiagonal for L_- and superdiagonal for L_+. Matrices with all elements $\{a_n\}_{n=1}^N$ on their sub- or superdiagonals non-vanishing and all other elements equal to zero are similar to a single Jordan block $J_{N+1}(0)$ with eigenvalue $\lambda = 0$:

$$\begin{pmatrix} 0 & a_1 & 0 & \cdots & 0 & 0 \\ 0 & 0 & a_2 & \cdots & 0 & 0 \\ \vdots & \vdots & \vdots & \ddots & \vdots & \vdots \\ 0 & 0 & 0 & \cdots & a_{N-1} & 0 \\ 0 & 0 & 0 & \cdots & 0 & a_N \\ 0 & 0 & 0 & \cdots & 0 & 0 \end{pmatrix} = Q^{-1}J_{N+1}(0)Q,$$

$$Q = \text{diag}\left(1, a_1, a_1a_2, \cdots, \prod_{k=1}^N a_k\right). \tag{32}$$

This is also immediately evident from the angular momentum operators: The ladder operators $L_\pm$ should only have a single eigenstate, namely "spin-up" resp. "spin-down", belonging to the eigenvalue $\lambda = 0$. Since for $|\gamma| = |v|$ the Hamiltonian is equivalent to $L_\pm$, with total angular momentum $N/2$, these configurations correspond to a degenerate eigenvalue $\lambda = 0$ which is an EP of order $N+1$. Under variation of γ it unfolds into $[(N+1)/2]$ eigenvalue pairs (and in case of $N+1$ odd, into an additional zero-eigenvalue) according to (28). The result is illustrated in figure 1. We note that although such a pairwise unfolding of an $(N+1)$th-order EP according to a square root law $\sqrt{v^2 - \gamma^2}$ with different scaling pre-factors n appears physically rather generic, it is mathematically very special. Typically an $(N+1)$th-order EP at $\lambda = 0$ unfolds under a small perturbation $|\epsilon| \ll 1$ into an $(N+1)-$ring $\lambda \approx e^{i\frac{2\pi k}{N+1}}\epsilon^{1/(N+1)}, \ k = 0, \ldots, N$ of non-degenerate eigenvalues. This follows simply from an effective equation of the type $\lambda^{N+1} \approx \epsilon$. Intuitively, one might expect the spectral behavior (28) with its decoupled square roots to result from a decomposition of H into $[\frac{N+1}{2}]$ second-order Jordan blocks rather than from a single $(N+1)$th-order Jordan block. The subject of the remaining sections will be to further clarify this specific (mathematically non-standard) spectral behavior of H.

In contrast to the simple analytical structure of the model and its complete solvability in case of vanishing interaction c, the situation changes drastically for non-vanishing interaction. In this case the spectrum of the non-Hermitian $\mathcal{PT}-$symmetric Hamiltonian (12) is most efficiently studied with the help of numerical and perturbational techniques. In the next section we will present some numerical

results for non-vanishing interaction. Qualitative aspects of these findings are explained analytically with the help of perturbational techniques in section 5.

4. Numerical results for non-vanishing interaction
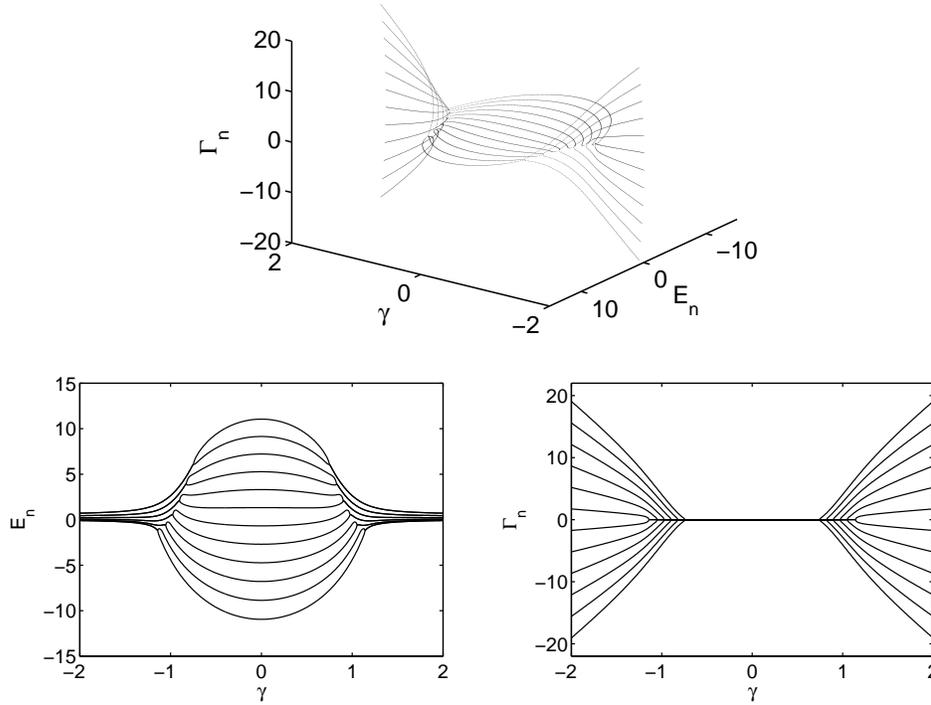
Figure 2. Real- and imaginary parts of the eigenvalues $\lambda_n = E_n - \mathrm{i}\Gamma_n$ of the Bose-Hubbard Hamiltonian (12) as a function of the non-Hermiticity γ for $v = 1$, $c = 0.1/N$ and $N = 11$ particles.

Figures 2 and 3 demonstrate the typical spectral behavior of a Hamiltonian (12) in dependence on the non-Hermiticity parameter γ for fixed weak and moderate interaction strength c. In the concrete example, the twelve eigenvalues of an $N = 11$ particle system are shown.

First we note that the non-vanishing interaction c reduces the symmetry of the spectrum: The symmetries with regard to sign changes of the complex coupling $\gamma \rightleftharpoons -\gamma$ and of the imaginary spectral components $\Gamma_n \rightleftharpoons -\Gamma_n$ are not altered. The first symmetry results from the fact that, regardless of the interaction, for symmetric modes it does not matter which of them is coupled to the source and which to the sink. Due to this $\gamma \rightleftharpoons -\gamma$ symmetry we can restrict our analysis to the parameter region $\gamma \geq 0$. The second symmetry (with regard to $\Gamma_n \rightleftharpoons -\Gamma_n$) is a direct implication of the Krein space symmetry (13) of H which causes non-real eigenvalues to occur always in complex conjugate pairs. The additional symmetry $E_n \rightleftharpoons -E_n$ present for $c = 0$ is lost in case $c \neq 0$. This is due to the fact that for $c \neq 0$ the square root branch points
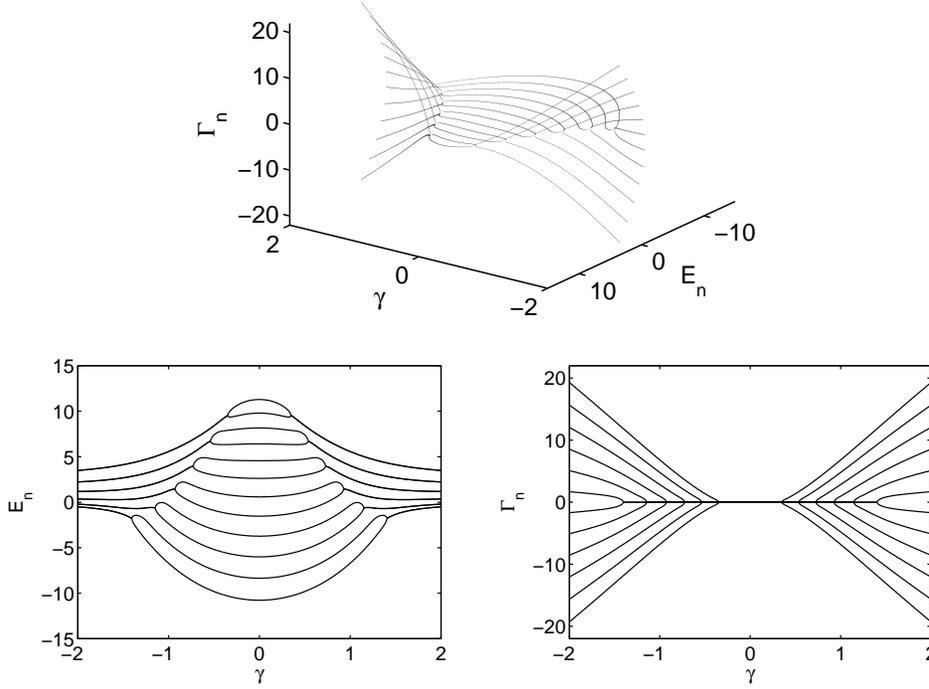
Figure 3. Real- and imaginary parts of the eigenvalues $\lambda_n = E_n - \mathrm{i}\Gamma_n$ of the Bose-Hubbard Hamiltonian (12) as a function of the non-Hermiticity γ for $v = 1$, $c = 0.5/N$ and $N = 11$ particles.
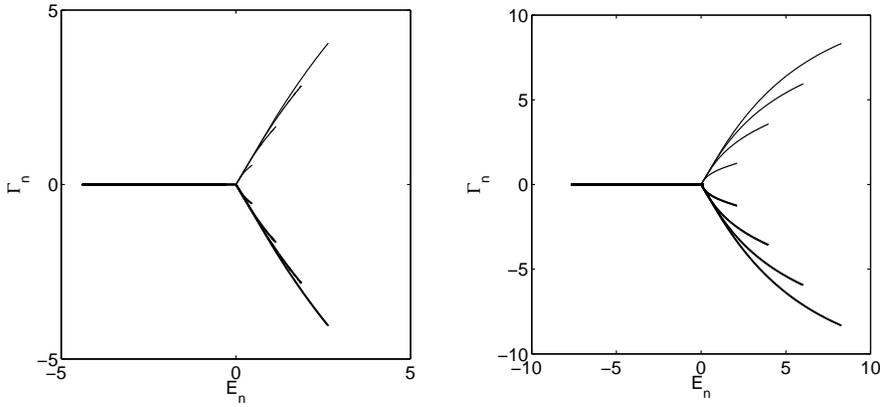
Figure 4. Trajectories of the complex energy eigenvalues $\lambda_n = E_n - \mathrm{i}\Gamma_n$ of the Bose-Hubbard Hamiltonian (12) as a function of c with $0 < cN < 0.1$ (left) and $0 < cN < 1$ (right), for $\gamma = v$, $N = 11$ particles.

(EPs) become shifted in different ways and do no longer coalesce in the parameter space $\mathcal{M} \cong \mathbb{R}^3 \ni (\gamma, v, c)$. For $|c| \ll |v|/N$, $\gamma^2 \approx v^2$ this behavior can be roughly described as an effective deformation of the spectral branches (28) of the type

$$\lambda_n(c) = a_n(c) + b_n(c)n\sqrt{v^2 - \gamma^2 - d_n(c)} \qquad a_n(0) = d_n(0) = 0, \quad b_n(0) = 1 \qquad (33)$$

which for $c \neq 0$ leads to

$$E_n = \operatorname{Re}\left[\lambda_n(c)\right] \neq -E_{-n} = -\operatorname{Re}\left[\lambda_{-n}(c)\right]. \qquad (34)$$

From figures 2 and 3 one clearly sees that for fixed $v = 1$ each of the two EPs of order twelve present in figure 1 at $\gamma = \pm v$ splits up into six second-order EPs with different positions $\gamma_n = \pm\sqrt{v^2 - d_n(c)}$. The fact that these special points are EPs is obvious from the graphics. One clearly sees, firstly, that these points are associated with transitions from real spectral branches to complex conjugate ones and that they are therefore branch points. Secondly, one observes that the lines which branch off from these points scale faster than linearly so that the points cannot be diabolical points which are connected with a linear scaling (see e.g. [22]).

For increasing $|c|$ the deviations from the spectrum at $c = 0$ also increase (compare figures 1, 2 and 3).

Subsequently, it is convenient to relabel the absolute values of the EP positions $|\gamma_n| =: \tilde{\gamma}_{k=\sigma(n)}$ in increasing order as

$$0 \leq \tilde{\gamma}_1 \leq \tilde{\gamma}_2 \leq \cdots. \qquad (35)$$

Furthermore, we dub the $(N + 1)$th-order EPs as mother EPs.

Complementary information about the unfolding of these mother EPs for non-vanishing interaction strength $c \neq 0$ can be gained by considering the behavior of the spectral branches at the former EP positions $|\gamma| = |v|$. For this purpose the trajectories of the twelve eigenvalues in the complex plane have been plotted for interaction strengths c varying in the intervals $0 < c \leq c_{\max} = 0.1/N$ and $0 < c \leq c_{\max} = 1/N$ (see figure 4). For definiteness we have chosen $v = 1$ so that the mother EP is localized at $\gamma = v = 1$. Obviously, for small $|c| \ll |v|/N$ the twelve eigenvalues form three groups where four eigenvalues behave qualitatively almost identical — moving along one of the three lines in the directions $\sim e^{-i\pi}, e^{-i\pi \pm i\frac{2\pi}{3}}$. This regular circle division with lines enclosing angles of $2\pi/3$ in the complex plane clearly indicates on an unfolding of the type

$$\lambda_{j,k} \sim (-f_j)^{1/3}e^{i\frac{2\pi k}{3}}c^{1/3}, \qquad k = 0, 1, 2, \qquad f_j \in \mathbb{R}^+, j = 1, 2, 3, 4 \qquad (36)$$

where three eigenvalues corresponding to the same f_j can be understood as a triplet. For larger values of c (see , e.g., the right side of figure 4) one eigenvalue of each triplet stays on the negative real axis, while the other two depart from their initial directions symmetrically with regard to the real axis as complex conjugate pairs.

The triplet splitting is less obvious from the spectral branches depicted in figures 2 and 3. Nevertheless, these plots also clearly show that at the position $\gamma = v = 1$ four purely real eigenvalues and four complex conjugate pairs of eigenvalues are present. Obviously, the triplet splitting is closely connected with the fact that for small $c \neq 0$ two of the second-order branch points (EPs) move to values $\tilde{\gamma}_5, \tilde{\gamma}_6 > 1$ yielding in this way four real eigenvalues at $\gamma = 1$, whereas the other four second-order EPs with $\tilde{\gamma}_1, \ldots, \tilde{\gamma}_4$ move to positions $0 < \tilde{\gamma}_k < 1$, what results in the four complex conjugate pairs at $\gamma = 1$.

Further numerical investigation shows that the triplet unfolding of the mother EP for $c \neq 0$ and $|\gamma| = |v|$ is a generic feature of the system (12) for arbitrary particle

number. In general, we find a splitting into $\left[\frac{N+1}{3}\right]$ eigenvalue triplets and $(N+1) \bmod 3$ single eigenvalues. In section 5, this unfolding behavior will be analytically explained with the help of perturbational techniques.
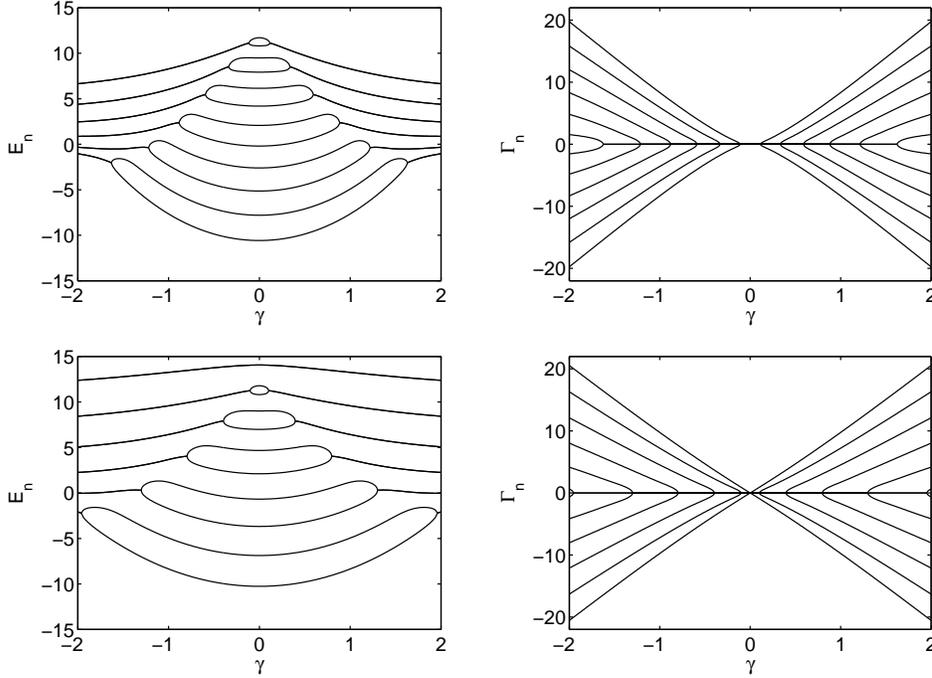
Figure 5. Real- and imaginary parts of the eigenvalues $\lambda_n = E_n - \mathrm{i}\Gamma_n$ of the Bose-Hubbard Hamiltonian (12) as a function of the non-Hermiticity γ for $v = 1$, $N = 11$ particles and $c = 1/N$ (upper figures) resp. $c = 2/N$ (lower figures).
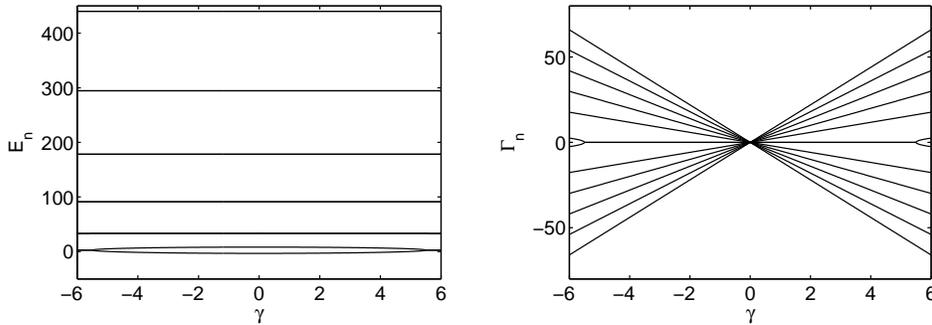
Figure 6. Real- and imaginary parts of the eigenvalues $\lambda_n = E_n - \mathrm{i}\Gamma_n$ of the Bose-Hubbard Hamiltonian (12) as a function of the non-Hermiticity γ for $v = 1$, $N = 11$ particles and $c = 80/N$.

After getting a rough qualitative understanding of the unfolding of the mother EPs at $|\gamma| = |v|$, $c = 0$ we turn now to the system behavior for intermediate
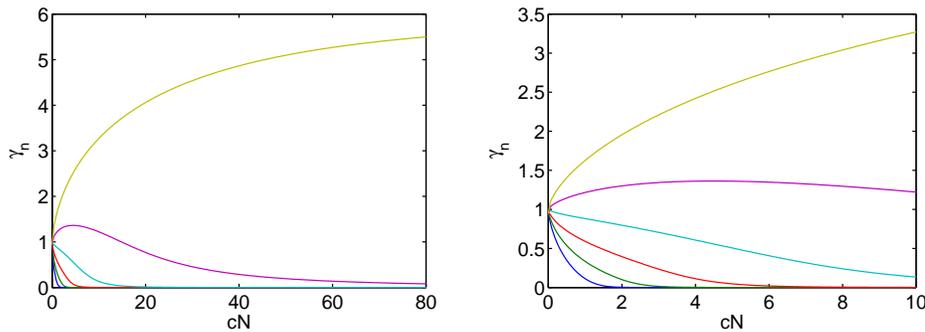
Figure 7. (Color online) EP positions in the $(c,\gamma)-$half-plane $\gamma \geq 0$ for fixed $v = 1$ and $N = 11$. The figure on the right is a magnification of the small cN region. The EP positions are numerically approximated as the smallest positive values of γ at which two formally degenerate resonance widths $\Gamma_{j,k}$ differ by more than 10^{-4}.

and large interaction strengths c. Figures 5 and 6 give an impression about the corresponding spectral behavior and figure 7 about the associated location of the EPs in the $(c,\gamma)-$half-plane. Obviously, the movement of the second-order EPs remains qualitatively the same for intermediate values of c: two of the six EPs connected with the mother EP at $\gamma = v = 1$ move away from $\gamma = 1$ to positions $\tilde{\gamma}_k > 1$, whereas the other four $\tilde{\gamma}_k$ remain located within the interval $(0,1) \ni \tilde{\gamma}_k$ and move to smaller γ. In the limit of $c \to \infty$ not only these four EPs tend asymptotically to the limiting value $\gamma = 0$ (see figures 6 and 7), but also the EP $\tilde{\gamma}_5$ originally located at $\gamma > 1$. The value $\gamma = 0$ itself is only reached at $c = \infty$, because for $c < \infty$ and $\gamma = 0$ the Hamiltonian H in (8) is a tridiagonal symmetric purely real matrix with non-vanishing elements on the superdiagonal. According to [61] (chapter 5, sections 36 and 37) such matrices have distinct (nondegenerate) eigenvalues.

Figure 5 clearly shows the shrinking of real spectral "bubbles" which are defined by the intervals $[-\tilde{\gamma}_k, \tilde{\gamma}_k]$, $k \leq 5$ for increasing c. The same fact is implicitly reflected in the EP behavior in the $(c,\gamma)-$half-plane (figure 7). The $\gamma-$positions of the EPs and with them the sizes of the real spectral "bubbles" tend only asymptotically to zero. By zooming into figures 5 and 7 one would observe still remaining real-energy regions for all spectral branches shown in figure 5. We note that the smallest of those regions $[-\tilde{\gamma}_1, \tilde{\gamma}_1]$ defines the sector of exact $\mathcal{PT}-$symmetry (all eigenvalues are purely real). For $c \to \infty$ this region together with the other intervals $[-\tilde{\gamma}_k, \tilde{\gamma}_k]$, $k \leq 5$ shrinks to zero width (see figure 6). The shrinkage effect for purely real branches and the widening of branches with complex conjugate eigenvalues is similar to the well known effect of eigenvalue complexification for strong-coupling regimes in Sturm-Liouville type $\mathcal{PT}-$symmetric models [53, 55].

In contrast to the EP accumulation $\tilde{\gamma}_k \to 0$, $k \leq 5$, for $c \to \infty$, the single EP pair $\pm\tilde{\gamma}_6$ tends asymptotically to the limiting values $\pm\tilde{\gamma}_6^{(\infty)} = \pm6$. This is the manifestation of a generic result which holds for systems with odd particle numbers N and which is derived by perturbation techniques in section 5.2. It states that for odd N and $c \to \infty$ the lowest two levels coalesce at EPs located at $\tilde{\gamma}_{\frac{N+1}{2}}^{(\infty)} = \pm v\frac{N+1}{2}$. In case of even N all EP positions tend asymptotically to $\gamma = 0$.

Let us restrict our attention (for symmetry reasons $\gamma \rightleftharpoons -\gamma$) to the region $\gamma \geq 0$. From the limiting locations of the EPs for $c \to 0$ and $c \to \infty$ and the numerical results for $c \in [0, \infty)$ we conclude that the second order EPs are located on two-dimensional hypersurfaces $\mathcal{V}_n = \{(\gamma, v, c) \in \mathcal{M} : \gamma = \gamma_n(v, c)\}$ in the three-dimensional parameter space $\mathcal{M} \ni (\gamma, v, c)$. For $c = 0$ these surfaces $\mathcal{V}_n$ coalesce at a common line $\bigcap_n \mathcal{V}_n = \{(\gamma, v, c) \in \mathcal{M} : \gamma = v, c = 0\}$. In the opposite limit of $c \to \infty$ all but one of the surfaces (in case of N odd) tend asymptotically to the plane $\mathcal{N}_0 = \{(\gamma, v, c) \in \mathcal{M} : \gamma = 0\}$. The remaining surface $\mathcal{V}_{\frac{N+1}{2}}$ asymptotically approaches the plane $\mathcal{N}_+ = \{(\gamma, v, c) \in \mathcal{M} : \gamma = v\frac{N+1}{2}\}$. Hence, the stratified manifold $\mathcal{V} \subset \mathcal{M}$ of EP degenerations for the present model comprises the two-dimensional surfaces $\mathcal{V}_n$ which intersect (coalesce) at the line $\bigcap_n \mathcal{V}_n$

$$\mathcal{V} = \bigcup_n \mathcal{V}_n \tag{37}$$

and its mirror images under the symmetry transformation $\gamma \rightleftharpoons -\gamma$.

Summarizing the numerical findings we conclude that although the influence of the particle interaction might stabilize some of the energy levels, i.e. it might shift the occurrence of their imaginary parts to higher values of the non-Hermiticity parameter γ, the position of the first EPs monotonically decreases with increasing interaction strength c. Therefore the interaction always shrinks the region of unbroken PT symmetry. In the limit of infinitely strong interaction even an arbitrarily small complex perturbation destroys the reality of the spectrum.

5. Perturbative results

In this section we will investigate some of the features of the spectrum of the Hamiltonian (12) for different limiting cases analytically using perturbational techniques.

At first we will focus on the unfolding of the $(N + 1)$th-order EP due to a weak particle interaction c. Since usual Rayleigh-Schrödinger perturbation theory breaks down for non-Hermitian Hamiltonians in the vicinity of EPs of the unperturbed operator, we resort to the Puiseux-Newton resp. Newton-polygon method [11, 40, 41], a perturbative technique for the roots of polynomials which works in the vicinity of degeneracies as well as around simple values. This method will allow us to analytically verify the triplet unfolding of the mother EP we found numerically in section 4.

Finally, in the second part of this section, we will use standard Rayleigh-Schrödinger perturbation to understand the behavior of the spectrum in the strong-interaction regime.

5.1. The limit of weak interaction

Here we are going to analyze the unfolding of the $(N + 1)$th-order EP when the interaction is switched on perturbatively, i.e., we consider the spectral behavior of the Hamiltonian (12) at the EP $\gamma = v$

$$H = 2v(L_x - iL_z) + 2cL_z^2 \tag{38}$$

for small interaction $0 \leq |c| \ll |v|/N$.

As a first step, we $SU(2)-$rotate the Hamiltonian (38) with the help of eq. (22) and $\theta = \pi/2$ into the more convenient form

$$
\begin{aligned}
\tilde{H} &= 2v(L_x - iL_y) + 2cL_y^2 \\
&= 2vL_- - \frac{c}{2}(L_+ - L_-)^2 \\
&=: 2vL_- - \frac{c}{2}\left(L_+^2 - L_0 + L_-^2\right), \qquad L_0 := L_+L_- + L_-L_+ . \quad (39)
\end{aligned}
$$

In the particle number (angular momentum l) representation this Hamiltonian has a band diagonal structure of the type

$$
\tilde{H} = \begin{pmatrix}
* & 0 & * & 0 & 0 & \cdots & \cdots & 0 & 0 \\
* & * & 0 & * & 0 & \cdots & \cdots & 0 & 0 \\
* & * & * & 0 & * & \cdots & \cdots & 0 & 0 \\
0 & * & * & * & 0 & \cdots & \cdots & 0 & 0 \\
\vdots & \ddots & \ddots & \ddots & \ddots & \ddots & \ddots & \vdots & \vdots \\
0 & 0 & \cdots & * & * & * & 0 & * & 0 \\
0 & 0 & \cdots & 0 & * & * & * & 0 & * \\
0 & 0 & \cdots & 0 & 0 & * & * & * & 0 \\
0 & 0 & \cdots & 0 & 0 & 0 & * & * & *
\end{pmatrix}, \qquad (40)
$$

where the second super- and subdiagonals are generated by the L_+^2 and L_-^2 terms and the diagonal by L_0. The perturbation matrix is an upper $3-$Hessenberg matrix, i.e. a matrix with only zero entries below the three subdiagonals (including the main diagonal). Therefore the results of [62] apply, where the unfolding of the eigenvalues of Jordan blocks $J_n(\lambda_0)$ under perturbations by general upper $k-$Hessenberg matrices has been analyzed. It has been shown that an nth-order EP typically splits into p rings of size k and one of size r (if $r \neq 0$), where $n = pk+r$, $p = \left[\frac{n}{k}\right]$ and $r = n \bmod p$. This means that for a small coupling parameter $|c| \ll |v|/N$ the EP will unfold as

$$
\begin{aligned}
\lambda_{q,j} &= a_q e^{i2\pi j/k} c^{1/k} + o(c^{1/k}), \qquad j = 0,\ldots,k-1 \quad q = 1,\ldots,p \\
\lambda_{0,l} &= a_0 e^{i2\pi l/r} c^{1/r} + o(c^{1/r}), \qquad l = 0,\ldots,r-1. \quad (41)
\end{aligned}
$$

The coefficients a_q are specific model dependent constants whose moduli $|a_q|$ define the scaling of the ring radii. The specific $n = pk+r$ splitting behavior generalizes the well known results for the generic case ($p = 1, r = 0$) where the degenerate eigenvalue at the EP splits into a single ring of size n, i.e. where (in suitable reparametrization) $\lambda^n = c$ holds, with the ring $\lambda = e^{i2\pi j/n} c^{1/n}$, $j = 0,\ldots,n-1$, of size n as obvious solutions. Applying the results of [62] to the unfolding of our EP configuration we expect the formation of $p = \left[\frac{N+1}{3}\right]$ rings of size $k = 3$ and possibly of a single ring of size $r = 1$ (single eigenvalue) or $r = 2$ (eigenvalue pair) depending on the concrete dimension $N + 1$ and $r = (N + 1) \bmod p$.

Subsequently, we present an explicit derivation of this behavior which makes use of the specific structure of our model. The analysis will be based on the characteristic polynomial of the matrix Hamiltonian $\tilde{H}$ (39) as function of the interaction strength c,

$$
\chi_{\tilde{H}}(\lambda, c) = \det\left(\lambda I - \tilde{H}\right) = -\sum_{k=0}^{M} p_{M-k}(c)\lambda^k, \qquad M := N + 1 \quad (42)
$$

which we will study with the help of the Newton-polygon technique [11,41]. This will allow us to derive the dominant fractional power μ of the unfolding $\lambda = a_0 c^\mu + o(c^\mu)$ of the $(N + 1)$th-order EP.

We start our analysis by noticing that the characteristic polynomial of any $\mathcal{PT}-$symmetric matrix Hamiltonian H has purely real coefficients. This follows straightforwardly from the fact that any $\mathcal{PT}-$symmetric operator can be represented as a purely real (possibly infinite dimensional) matrix [63].

The coefficients $p_{M-k}(c)$ in (42) can be recursively obtained with the help of the Le Verrier-Faddeev method [39] as

$$p_k = -\frac{1}{k}\sum_{j=1}^{k} s_j p_{k-j}, \quad k = 1, \dots, M, \tag{43}$$

$$s_k := \text{Tr}(\tilde{H}^k), \qquad p_0 = -1.$$

For our purpose it is sufficient to extract the structure of the coefficients $p_k(c)$ as polynomials in c. As basic input we first derive the corresponding traces $s_k(c) = \text{Tr}(\tilde{H}^k)$. These traces act in the angular momentum representation (7) or, equivalently, in the monomial representation (9). This means that only terms in $\tilde{H}^k$ contribute to $\text{Tr}(\tilde{H}^k)$ which leave the angular momentum mode number m, and with it the monomial power, unchanged. Hence it will hold , e.g., $\text{Tr}(L_\pm^k) = 0 \ \forall k \in \mathbb{Z}^+$, i.e. $k > 0$, as well as $\text{Tr}(L_+^k L_-^j) = 0 \ \forall k \neq j \in \mathbb{Z}^+$, but $\text{Tr}(L_+^k L_-^k) \neq 0$. In order to extract the power structure of $s_k(c)$ in c we may relate to $L_\pm$ their auxiliary commutative symbols $L_+ \approx \xi$, $L_- \approx \xi^{-1}$. The terms $\tilde{H}^k$ can then be associated with the multinomials

$$\tilde{H}^k \approx \left[v\xi^{-1} + c(\xi - \xi^{-1})^2 \right]^k$$

$$\approx \sum_{l=0}^{k} \binom{k}{l} v^{k-l}\xi^{l-k}c^l \sum_{i=0}^{2l} \binom{2l}{i}(-1)^i \xi^{2(i-l)} \tag{44}$$

(we omitted the irrelevant pre-factors 2 and $-1/2$ in front of v and c) where only the constant ξ^0-terms will contribute to the trace $\text{Tr}(\tilde{H}^k)$. With the notation $j := i - l$ we find the ξ^0-terms as $\xi^0 = \xi^{l-k+2j}$. Combining the corresponding constraint $k - l = 2j$ with the inequalities $k \geq l \geq 0$, $2l \geq i \geq 0$ one obtains $j \leq l = k - 2j$ and, hence, the condition $k \geq 3j$ or $j \leq \left[\frac{k}{3}\right]$.

As result, we find the structure of the traces as

$$s_k(c,v) = \text{Tr}(\tilde{H}^k) = \sum_{j=0}^{\left[\frac{k}{3}\right]} a_j^{(k)} c^{k-2j} v^{2j}. \tag{45}$$

The constant coefficients $a_j^{(k)}$ depend only on k and the particle number N (resp. the angular momentum l) and can be calculated with the help of general trace formulae for polynomials of angular momentum operators as discussed, e.g., in [64]. In our subsequent qualitative analysis we are only interested in the behavior of $s_k(c,v)$ as polynomial in c so that the concrete values of the non-vanishing coefficients $a_j^{(k)}$ are irrelevant.

The trace formula (45) allows us to prove the following

Theorem. *The coefficients p_k have the structure*

$$p_k = \sum_{j=0}^{\left[\frac{k}{3}\right]} d_j^{(k)} c^{k-2j} v^{2j} \tag{46}$$

where $d_j^{(k)}$ are real constants which in general do not vanish.

Proof. The theorem is true for $k = 0$ and $k = 1$ where (43) and (45) imply

$$p_0 = -1, \qquad p_1 = -p_0 s_1 = s_1 = a_0 c^1. \qquad (47)$$

From (43) and (45) one finds (46) by induction:

$$
\begin{aligned}
p_{n+1} &= -\frac{1}{n+1} \sum_{k=1}^{n+1} s_k p_{n+1-k} \\
&= -\frac{1}{n+1} \sum_{k=1}^{n+1} \sum_{l=0}^{\left[\frac{k}{3}\right]} \sum_{j=0}^{\left[\frac{n+1-k}{3}\right]} a_l^{(k)} d_j^{(n+1-k)} c^{n+1-2(l+j)} v^{2(l+j)} \quad (48) \\
&= \sum_{r=0}^{\left[\frac{n+1}{3}\right]} b_r^{(n+1)} c^{n+1-2r} v^{2r} \qquad (49)
\end{aligned}
$$

$$b_r^{(n+1)} := -\frac{1}{n+1} \sum_{k=1}^{n+1} \sum_{l=0}^{\left[\frac{k}{3}\right]} \sum_{j=0}^{\left[\frac{n+1-k}{3}\right]} a_l^{(k)} d_j^{(n+1-k)} \delta_{r,l+j}.$$

In passing from (48) to (49) we used the fact that the total summation in (48) goes over the three-dimensional discrete volume $\Omega = \{k, l, j : 1 \le k \le n+1, 0 \le l \le \left[\frac{k}{3}\right], 0 \le j \le \left[\frac{n+1-k}{3}\right]\}$ and that Ω is recovered by slicing it along fixed $r = l + j$ and summing over the two-dimensional slices. $\qquad\qquad$ $\square$

Summarizing the above results we conclude that for a given index k it is sufficient to use the single index j as basic counting index, whereas the power of c in the polynomial terms is defined by the derived value l according to the relation:

$$l = k - 2j \qquad j \le \left[\frac{k}{3}\right]. \qquad (50)$$

As an illustration we list the $c-$dependence of the first six non-trivial coefficients p_k, $k = 1, \ldots, 6$ of the characteristic polynomial $\chi_{\tilde{H}}(\lambda, c)$. According to (46) these coefficients contain terms of the following $c^l v^{2j}-$monomial types

$$
\begin{array}{llll}
k = 1 & j = 0, & l = 1, & c^1 v^0 \\
k = 2 & j = 0, & l = 2, & c^2 v^0 \\
k = 3 & j = 0, & l = 3, & c^3 v^0 \\
       & j = 1, & l = 1, & c^1 v^2 \\
k = 4 & j = 0, & l = 4, & c^4 v^0 \\
       & j = 1, & l = 2, & c^2 v^2 \\
k = 5 & j = 0, & l = 5, & c^5 v^0 \\
       & j = 1, & l = 3, & c^3 v^2 \\
k = 6 & j = 0, & l = 6, & c^6 v^0 \\
       & j = 1, & l = 4, & c^4 v^2 \\
       & j = 2, & l = 2, & c^2 v^4.
\end{array}
\qquad (51)
$$

With the concrete monomial terms (51) at hand, it is now an easy task to obtain the leading (dominating) exponent μ_1 in the power series expansion

$$\lambda(c) = e_1 c^{\mu_1} + e_2 c^{\mu_2} + o(c^{\mu_2}), \quad 0 < \mu_1 < \mu_2 < \cdots, \quad e_i \ne 0 \qquad (52)$$

for small $|c| \ll |v|/N$. The method that we use is known as Puiseux-Newton diagram technique or Newton-polygon technique [11, 40, 41] and can be summarized as follows. One starts by substituting the ansatz (52) with still unknown exponents μ_i and coefficients e_i into the characteristic polynomial (42)

$$
\begin{aligned}
\chi_{\tilde{H}}[\lambda(c), c] \quad &= \lambda^M - p_1(c)\lambda^{M-1} - \cdots - p_{M-1}(c)\lambda - p_M(c) = 0 \\
&= (e_1 c^{\mu_1} + \cdots)^M - (f_{M-1} c^{a_{M-1}} + \cdots)(e_1 c^{\mu_1} + \cdots)^{M-1} - \\
&\quad - \cdots - (f_1 c^{a_1} + \cdots)(e_1 c^{\mu_1} + \cdots) - (f_0 c^{a_0} + \cdots) = 0.
\end{aligned}
\tag{53}
$$

The dots in the various terms denote contribution of higher powers in c. For later convenience the lowest $c-$powers in the coefficients p_k are numbered in reversed order as

$$
p_k(c) = f_{M-k} c^{a_{M-k}} + o(c^{a_{M-k}}).
\tag{54}
$$

Since $\chi_{\tilde{H}}[\lambda(c), c]$ as polynomial in c has to vanish, $\chi_{\tilde{H}}[\lambda(c), c] = 0$, it should contain at least two terms in each power in c so that these terms can compensate one another. Taking into account that terms in the lowest power in c are the most dominating ones, one has to search for these lowest-power-terms and to fix the still undefined μ_i in such a way that these terms compensate. After fixing the minimal μ_1 one repeats the process for the next greater μ_2 and so on. In this way one can iteratively obtain the series expansion (52) up to any required precision. The validity of the perturbative results is of course limited by the finite convergence radius of the perturbation series (52).

Returning to (53), one sees that μ_1 as minimal exponent should be defined from the monomials

$$
e_1^M c^{M\mu_1}, \; f_{M-1} e_1^{M-1} c^{a_{M-1}+(M-1)\mu_1}, \; f_{M-2} e_1^{M-2} c^{a_{M-2}+(M-2)\mu_1}, \ldots, f_0 c^{a_0}
\tag{55}
$$

by pairwise identifying their powers

$$
a_k + k\mu_{j,k} = a_j + j\mu_{j,k}, \qquad j \neq k, \quad j, k = 0, \ldots, M.
\tag{56}
$$

In order to single out the relevant values of μ_1 one associates to each power $a_k + k\mu_{j,k}$ a point $A_k = (k, a_k)$ in the $(k, a_k)-$plane so that

$$
\mu_{j,k} = -\frac{a_k - a_j}{k - j}
\tag{57}
$$

is just the sign-inverted slope of the line connecting the points A_j and A_k. As shown, e.g., in [11,40,41], the possible values of μ_1 can then be identified with those $\mu_{j,k}$ whose lines form the lower boundary of the convex hull of the points A_k. The corresponding graph is the so-called Newton polygon. Examples are depicted in figure 8. Points above this lower boundary of the convex hull will only contribute to higher order approximations.

The coefficients e_1 in the series expansion (52) can be obtained from reduced polynomials which are built from those leading-order terms of the characteristic polynomial (53) which correspond to points A_k located on the same lines of the Newton-polygon. In general, the lines comprise more than two points as it is visible, e.g., in figure 8. Here for $N = 5$ the $(\mu_1 = 1/3)-$line comprises three points and for $N = 10$ the $(\mu_1 = 1)-$line also comprises three points and the $(\mu_1 = 1/3)-$line four points.

Applying the described Puiseux-Newton technique to our concrete characteristic polynomial we read off from eq. (46) that the lowest $c-$powers in the coefficients $p_k(c)$
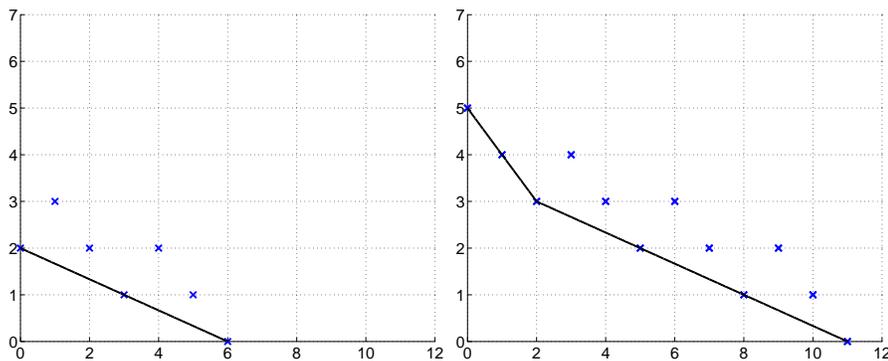
Figure 8. Puiseux-Newton-diagram for $N = 5$ particles (left) and $N = 10$ particles (right).

have the form $d^{(k)}_{\left[\frac{k}{3}\right]} c^{k-2\left[\frac{k}{3}\right]}$. With $M = N + 1$ and the reverse numbering (54) we find the relevant points A_k in the $(k, a_k)-$plane as

$$A_{N+1-k} = \left(N + 1 - k, k - 2\left[\frac{k}{3}\right]\right), \qquad k = 0, \dots, N + 1. \tag{58}$$

In case of $N = 5$ this gives, for example, the seven points

$$A_0 = (0, 2), \quad A_1 = (1, 3), \quad A_2 = (2, 2), \quad A_3 = (3, 1)$$
$$A_4 = (4, 2), \quad A_5 = (5, 1), \quad A_6 = (6, 0) \tag{59}$$

which are depicted in the left graphics of figure 8. Both of the two graphics in this figure show a typical modulo-three-ratchet-structure of the points A_k. The lower boundary of the convex hull of these points is always formed by one (long) line of slope $-1/3$ (and corresponding $\mu_1 = 1/3$) which connects $\left[\frac{N+1}{3}\right] + 1$ points A_k and possibly a second (short) line of slope -1 (and $\mu_1 = 1$) which connects the first two or three leftmost points. We arrive at the result that in our model only dominant eigenvalue scalings of the type

$$\lambda \propto c^{1/3}, \qquad \lambda \propto c \tag{60}$$

are possible. Obviously, these eigenvalues will form rings of size three (triplets) and of size one (single eigenvalues). The specific size-one rings can be considered as atypical cases in the scheme of [62]. They can be attributed to the specific substructure of the Hessenberg type perturbation matrix. Moreover these $\lambda \sim c$ terms can be identified as higher-order corrections — what is clearly visible by setting $c^{1/3} =: \epsilon$ so that $c = \epsilon^3$. This is a specific output of the Newton-diagram technique which yields the dominant terms for all roots of a polynomial. In our concrete case this means that the 3$-$rings correspond to dominant lowest-order scaling $c^{1/3}$, whereas the single eigenvalues remain unperturbed in this lowest order. Their dominant terms start only with the higher-order $\lambda \sim c$ contributions.

Let us now illustrate the general theoretical results by more explicit calculations for models with $N = 5$ and $N = 10$ particles. For the $N = 5$ model the corresponding

Hamiltonian has the form

$$H = \begin{pmatrix} -5\mathrm{i}\gamma + \frac{25}{2}c & \sqrt{5}v & 0 & 0 & 0 & 0 \\ \sqrt{5}v & -3\mathrm{i}\gamma + \frac{9}{2}c & 2\sqrt{2}v & 0 & 0 & 0 \\ 0 & 2\sqrt{2}v & -\mathrm{i}\gamma + \frac{1}{2}c & 3v & 0 & 0 \\ 0 & 0 & 3v & \mathrm{i}\gamma + \frac{1}{2}c & 2\sqrt{2}v & 0 \\ 0 & 0 & 0 & 2\sqrt{2}v & 3\mathrm{i}\gamma + \frac{9}{2}c & \sqrt{5}v \\ 0 & 0 & 0 & 0 & \sqrt{5}v & 5\mathrm{i}\gamma + \frac{25}{2}c \end{pmatrix}. \quad (61)$$

In case of $\gamma = v$ the characteristic polynomial reads

$$0 = \det(H - \lambda I)$$
$$= \lambda^6 - 35c\lambda^5 + \frac{1743}{4}c^2\lambda^4 + \left(-\frac{4645}{2}c^3 + 448v^2c\right)\lambda^3$$
$$+ \left(\frac{82831}{16}c^4 - 6112v^2c^2\right)\lambda^2 + \left(-\frac{58275}{16}c^5 + 27280v^2c^3\right)\lambda$$
$$+ \frac{50625}{64}c^6 - 30600v^2c^4 + 6400v^4c^2. \quad (62)$$

Obviously, $\lambda = 0$ is the only root for $c = 0$. For $|c| > 0$ the coordinates of the points (59) in the Puiseux-Newton diagram are given by the exponent of λ and the minimal exponent of c of each summand. Under the conditions described above one finds one straight line with the slope $-1/3$ and associated $\mu_1 = 1/3$. The three summands corresponding to the three points on this straight line must compensate each other

$$6400c^2v^4 + 448v^2c\lambda^3 + \lambda^6 = 0, \quad \lambda = e_1c^{1/3} + \dots. \quad (63)$$

This yields two solution triplets for the coefficient e_1:

$$e_1^{(1)} = -\sqrt[3]{14.77}v^{\frac{2}{3}}, \qquad e_1^{(4)} = -\sqrt[3]{433.23}v^{\frac{2}{3}},$$
$$e_1^{(2)} = \sqrt[3]{14.77}v^{\frac{2}{3}}e^{\mathrm{i}\frac{\pi}{3}}, \qquad e_1^{(5)} = \sqrt[3]{433.23}v^{\frac{2}{3}}e^{\mathrm{i}\frac{\pi}{3}},$$
$$e_1^{(3)} = \sqrt[3]{14.77}v^{\frac{2}{3}}e^{-\mathrm{i}\frac{\pi}{3}}, \qquad e_1^{(6)} = \sqrt[3]{433.23}v^{\frac{2}{3}}e^{-\mathrm{i}\frac{\pi}{3}}. \quad (64)$$

Figure 9 shows the real parts (left graphics) and the imaginary parts (right graphics) of the numerically evaluated eigenvalues of the Hamiltonian (61) for a small interaction strength $c = 0.1/N$. On the line $\gamma = v$ we find two pairs of complex conjugate eigenvalues with positive real parts and two purely real negative eigenvalues, in perfect agreement with the qualitatively predictions of the first order perturbation coefficients (64).

The numerically obtained eigenvalue trajectories in the complex plane for $c \in (0,1)$ and fixed $\gamma = v$ are shown in figure 10. For small $c \neq 0$ we find again the typical $3-$rings. Their radii are given by the two different absolute values of the coefficients (64). For larger values of c the cubic-root-behavior becomes deformed by higher order corrections what is clearly visible as a deviation from the straight lines $\sim e^{-\mathrm{i}\pi \pm \mathrm{i}\frac{2\pi}{3}}$. We note that the exact trajectories can be approximated in terms of a series expansion with arbitrary precision. Such series expansions are well defined over parameter regions which lie within the convergence radius of the series and break down when the next located algebraic singularity (branch point, EP) is reached. (The distance to the next EP defines the convergence radius (see, e.g., [65]).)

Let us now turn to the model with $N = 10$ particles. The corresponding Puiseux-Newton-diagram in figure 8 shows again the typical modulo-three-ratchet-structure. The two straight lines which form the lower boundary of the convex hull of the point
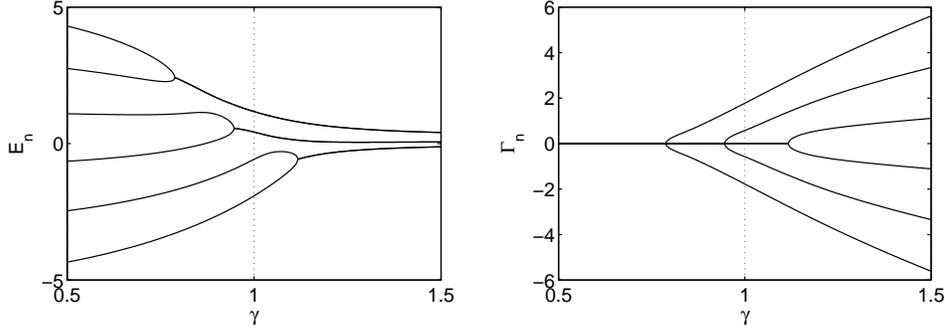
Figure 9. Real- and imaginary parts of the eigenvalues $\lambda_n = E_n - \mathrm{i}\Gamma_n$ of the Bose-Hubbard Hamiltonian (12) as a function of the non-Hermiticity γ for $v = 1$, $N = 5$ particles and $c = 0.1/N$.
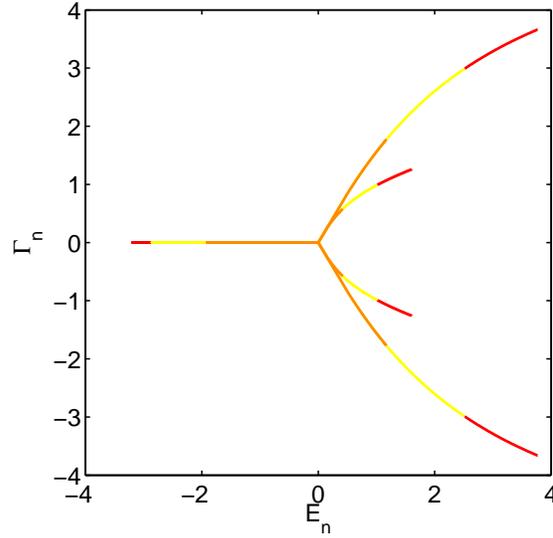
Figure 10. (Color online) Trajectories of the complex energy eigenvalues $\lambda_n = E_n - \mathrm{i}\Gamma_n$ of the Bose-Hubbard Hamiltonian (12) as a function of c with $0 < cN < 1$ (red), $0 < cN < 0.5$ (yellow) and $0 < cN < 0.1$ (orange), for $\gamma = v$, $N = 5$ particles.

set have slopes $-1/3$ and -1 so that the 11th-order EP unfolds with dominant scaling powers $\mu_1^{(1)} = 1/3$ and $\mu_1^{(2)} = 1$, i.e. as $\lambda \sim c^{1/3}$ and $\lambda \sim c$. Reinserting these solutions into the corresponding characteristic polynomial yields one ninth-order equation for the coefficient e_1 in $\lambda \approx e_1 c^{1/3}$. This ninth-order equation reduces to a cubic equation in e_1^3 and gives the three different values $|e_1|$ as scaling parameters (ring radii) of the three triplets which comprise the first nine coefficients $e_1^{(1)}, \ldots, e_1^{(9)}$. The result is similar to eq. (64) only with three triplets instead of two. The quadratic equation
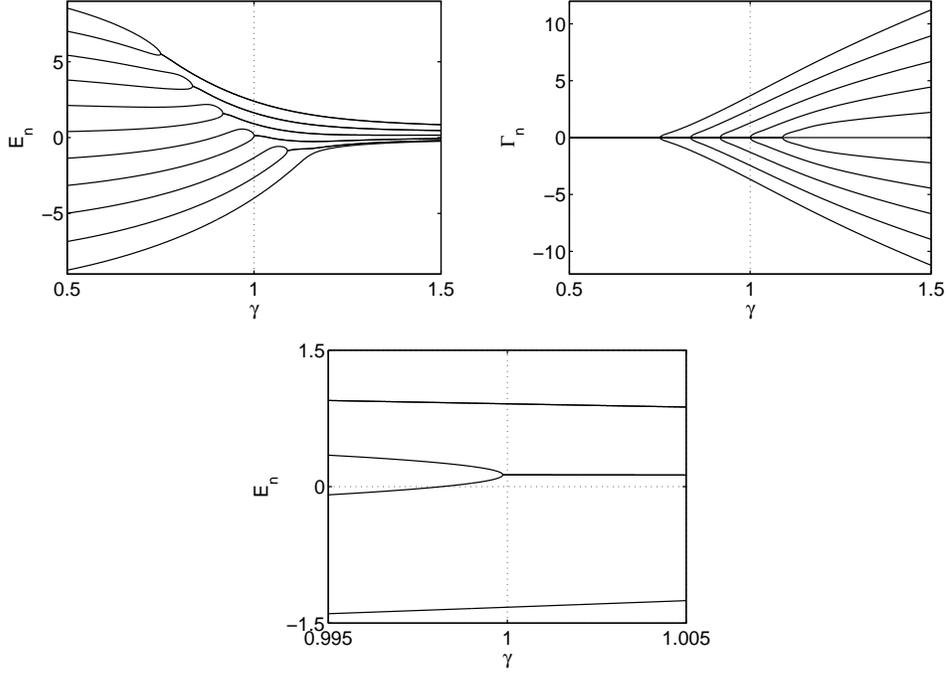
Figure 11. Real- and imaginary parts of the eigenvalues $\lambda_n = E_n - \mathrm{i}\Gamma_n$ of the Bose-Hubbard Hamiltonian (12) as a function of the non-Hermiticity γ for $v = 1$, $N = 10$ particles and $c = 0.1/N$. The lower figure shows a magnification of the real parts near the central EP.
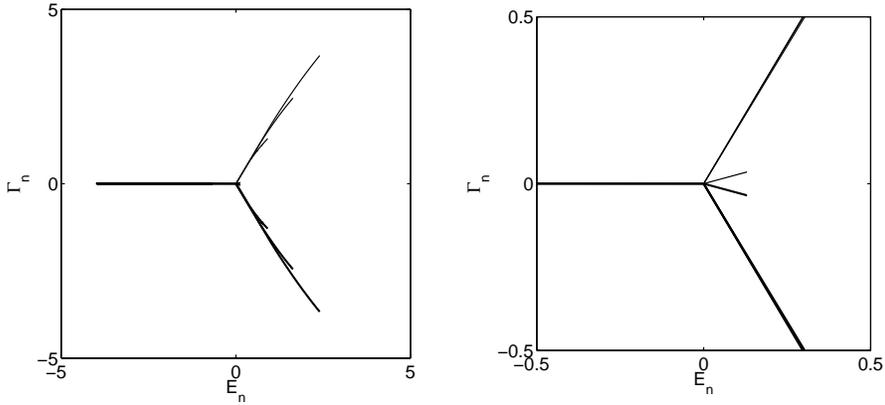
Figure 12. Trajectories of the complex energy eigenvalues $\lambda_n = E_n - \mathrm{i}\Gamma_n$ of the Bose-Hubbard Hamiltonian (12) as a function of c with $0 < cN < 0.1$, for $\gamma = v$, $N = 10$ particles and a magnification of the innermost region (right).

for the remaining two coefficients $e_1^{(10)}, e_1^{(11)}$ in the linear scaling law $\lambda \approx e_1 c$ is easily derived by computer algebra and takes the explicit form

$$- 46423756800e_1^2 + 2410418995200e_1 - 33581039616000 = 0. \qquad (65)$$

It yields the coefficients

$$e_1 = \frac{145304}{5597} \pm \sqrt{\left(\frac{145304}{5597}\right)^2 - \frac{4048640}{5597}} \approx 26 \pm 7\mathrm{i}. \qquad (66)$$

Real and imaginary part of the spectrum as well as the unfolding of the 11th-order EP at $c = 0$ and $\gamma = v = 1$ are shown in figures 11 and 12. Clearly visible in figure 12 are the three $3-$rings and the two linearly scaling single eigenvalues. Obviously, eigenvalue shifts induced by the linear scaling are much smaller than the shifts of the $3-$rings. In figures 11 and 12 these higher-order ($\lambda \sim c$) corrections are only visible in the zoomed graphics. In leading $c^{1/3}-$order approximation, the EP related to the $\lambda \sim c$ branches remained fixed at the original position $\gamma = v = 1$.

Summarizing we conclude that for arbitrary particle number N the Newton-diagram at the $(N+1)$th-order EP shows a modulo-three-ratchet-structure with regard to the unfolding due to increasing interaction strength c — like in figure 8. For non-vanishing c the EP unfolds into $\left[\frac{N+1}{3}\right]$ eigenvalue triplets forming regular $3-$rings in the complex plane with dominant scaling behavior of the type $c^{1/3}$ for $|c| \ll |v|/N$. The remaining $(N + 1) \bmod 3$ single eigenvalues depend linearly on c. Furthermore we find for small interaction strength c and an original $(N + 1)$th-order EP at $|\gamma| = |v|$ that roughly 2/3 of the occurring second-order EPs are located in parameter regions $0 < |\gamma| < |v|$ and roughly 1/3 in the region $|v| < |\gamma|$ what confirms the numerical results of section 4.

It remains to emphasize that the unfolding of $(N+1)$th-order EPs into triplets (for $\gamma^2 = v^2$) has its origin in the effective $3-$Hessenberg form of the perturbation matrix (39), (40). This suggests to reinterpret the square-root spectrum of the exactly solvable $(c = 0)-$model from section 3 as EP unfolding under perturbation by a $2-$Hessenberg matrix. Indeed, representing the Hamiltonian (19) as

$$H = 2v(L_x - iL_z) - 2i\Delta L_z \qquad\qquad \Delta := \gamma - v \qquad (67)$$

and performing an $SU(2)$ rotation as for (39) it takes the structure

$$\tilde{H} = 2vL_- - \Delta(L_+ - L_-). \qquad (68)$$

Due to the fact that L_- is of Jordan block type the Hessenberg perturbation theory of [62] is applicable. The perturbation matrix $\Delta(L_+ - L_-)$ has non-vanishing entries only on the first sub- and superdiagonals and it is therefore of $2-$Hessenberg type. According to [62] the $(N + 1)$th-order EP at $\Delta = 0$ unfolds then under this $2-$Hessenberg type perturbation into $\left[\frac{N+1}{2}\right]$ eigenvalue pairs and, for N even, into one additional single eigenvalue. Obviously, this prediction is in complete agreement with the exact result (28) for the spectrum which shows a square root (pairwise) unfolding of the mother EP and an additional single eigenvalue $\lambda = 0$ in case of even N.

The EP unfolding according to the Hessenberg perturbation type is straightforwardly extendable to Hamiltonians with $\gamma = v$ and higher-order perturbations in L_z

$$H = 2v(L_x - iL_z) + cL_z^k \qquad\qquad k \geq 2. \qquad (69)$$

In this case an $SU(2)$ rotation leads to

$$\tilde{H} = 2vL_- + \left(-\frac{i}{2}\right)^k c(L_+ - L_-)^k. \qquad (70)$$
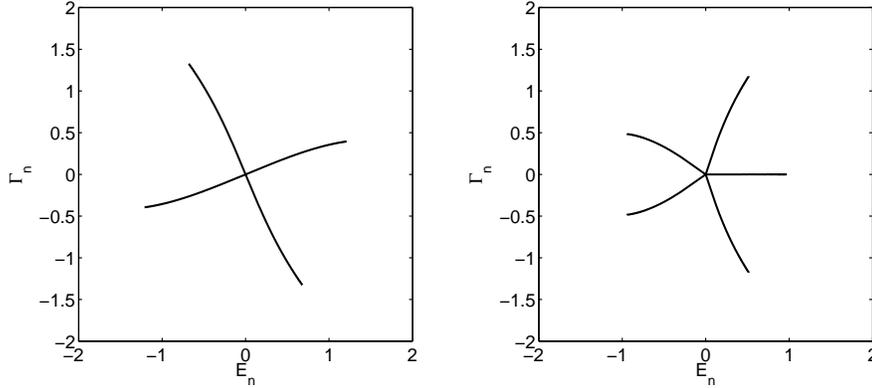
Figure 13. Eigenvalue trajectories of a $(N = 4)-$particle Bose-Hubbard Hamiltonian (69) with fixed $v = 1$ for $k = 3$ and $0 < c < 0.1/N^2$ (left, 4$-$ring) and for $k = 4$ and $0 < c < 0.1/N^3$ (right, 5$-$ring).

For $1 \leq k \leq N$ the perturbation matrix $(L_+ - L_-)^k$ is of $(k+1)-$Hessenberg type so that the $(N+1)$th-order EP will unfold into $[\frac{N+1}{k+1}]$ eigenvalue rings of size $k+1$ and $r = (N + 1) \mod (k + 1)$ eigenvalues which will be grouped in one or several smaller rings. Figure 13 shows the EP unfolding for $(N = 4)-$particle Hamiltonians (69) with $k = 3$ and $k = 4$, small c and fixed $\gamma = v = 1$. Clearly visible are the 4$-$ring and 5$-$ring eigenvalue structures. For $k \geq N$ also the lowest left matrix element becomes, in general, nonvanishing $H_{N+1,1} \neq 0$ so that for these k the mother EP will unfold into a single $(N + 1)-$ring of eigenvalues.

5.2. The limit of strong interaction

To understand the limit of strong interaction analytically, we can apply ordinary perturbation theory with γ and v being the small parameters:

$$H = \underbrace{2cL_z^2}_{H_0} \underbrace{-2\mathrm{i}\gamma L_z + 2vL_x}_{H_1}. \tag{71}$$

In general the eigenstates of H_0 are doubly degenerate, which can be seen in the standard basis (7)

$$2cL_z^2|l, \pm m_z\rangle = 2cm_z^2|l, \pm m_z\rangle, \tag{72}$$

with $l = \frac{N}{2}$. An exclusion is the eigenstate with $m_z = 0$ in a system with even particle number N. This state is not degenerate.

In lowest-order approximation, the perturbed degenerate energy levels are given as

$$E \simeq E_0 + E_1, \tag{73}$$

where the corrections E_1 can be calculated from the perturbation matrix

$$W = \langle l, m_z|H_1|l, m_z'\rangle \qquad m_z, m_z' = \pm|m_z|. \tag{74}$$

We start with even particle numbers N. In this case the matrix W is diagonal and the energy corrections read

$$E_1 = -2\mathrm{i}\gamma m_z. \tag{75}$$

Obviously, the state $m_z = 0$ remains unperturbed in lowest order approximation.

For odd particle numbers N the correction (75) holds as well, except in the case of $|m_z| = 1/2$ where the perturbation matrix is nondiagonal

$$W = \begin{pmatrix} -\mathrm{i}\gamma & v\frac{N+1}{2} \\ v\frac{N+1}{2} & \mathrm{i}\gamma \end{pmatrix}. \tag{76}$$

The eigenvalues of this matrix are

$$E_1 = \pm\sqrt{v^2\left(\frac{N+1}{2}\right)^2 - \gamma^2} \tag{77}$$

and we see that there occur two second-order EPs at $\gamma = \pm\frac{N+1}{2}v$. The corrections E_1 for the states $|m_z| = \frac{1}{2}$ are purely real for $|\gamma| < |v|\frac{N+1}{2}$ and purely imaginary for $|\gamma| > |v|\frac{N+1}{2}$.

The exact spectrum (28) for $c = 0$ and the numerical studies for $c \neq 0$ show that pairwise complex conjugate eigenvalues of H occur for large values of $|\gamma|$. In connection with the purely imaginary perturbative corrections E_1 for states with $|m_z| > 1/2$ this implies that for large $|c| \gg |v|/N$ all EPs involving these states must have tended to $\gamma \to 0$.

Summarizing we conclude that in the limit $c \to \infty$ there exists one zero-eigenvalue state with $m_z = 0$ for N even and a pair of real eigenvalues for states $|m_z| = 1/2$ in the parameter region $|\gamma| < |v|\frac{N+1}{2}$ of a model with N odd. All remaining eigenvalues come as complex conjugate pairs.

Therefore these perturbative results prove the numerical observations of section 4, that in the limit of ultra-strong interaction all EPs of an $N-$even model are located at $\gamma = 0$, whereas in an $N-$odd model two of the EPs can be found at $\gamma = \pm v\frac{N+1}{2}$.

6. Conclusion and Outlook

We studied the spectrum of a non-Hermitian $\mathcal{PT}-$symmetric two-mode Bose-Hubbard Hamiltonian, a system modeling an $N-$particle Bose-Einstein condensate in a double well potential containing a sink in one of the wells and a source of equal strength in the other. While for vanishing particle interaction there exists only one pair of EPs of order $N+1$, the interplay of non-Hermiticity and particle interaction leads to a characteristic unfolding of these EPs into $3-$rings of eigenvalues and the occurrence of a series of EPs of order two. This numerically observed scenario has been analytically understood using the Puiseux-Newton perturbation technique. Furthermore the case of strong particle interaction was described by ordinary Rayleigh-Schrödinger perturbation theory.

Further investigations concerning, e.g., the positions of the EPs as well as their influence on the system dynamics remain tasks for future research.

Another challenge is the investigation of the large N limit of the present model, resp. the so called mean-field approximation. In the Hermitian case this mean-field approximation is usually achieved by replacing the bosonic field operators by c-numbers, the condensate wave functions, yielding the nonlinear Schrödinger equation resp. Gross-Pitaevskii equation. This approach is closely related to a classicalization.

In a number of recent papers consequences of the classical nature of the mean-field approximation are discussed and semiclassical aspects are introduced [33,35,36,66–68]. For a two-mode system even the eigenenergies and eigenstates of the many particle system could be reconstructed approximately from the mean-field system in a semiclassical approximation with astonishing accuracy [69]. While there are some investigations concerning an heuristically introduced non-Hermitian generalization of discrete nonlinear Schrödinger equations [37,70–74] a careful derivation of a mean-field approximation starting from a non-Hermitian many particle system was lacking in the past and will be the subject of a separate paper [75].

Acknowledgments

References

[1] J. Okolowicz, M. Ploszajczak, and I. Rotter, Phys. Rep. **374** (2003) 271.
[2] C. M. Bender and S. Boettcher, Phys. Rev. Lett. **80**, 5243 (1998), physics/9712001.
[3] C. M. Bender, S. Boettcher and P. N. Meisinger, J. Math. Phys. **40**, 2201 (1999), quant-ph/9809072.
[4] M. Znojil, Phys. Lett. **A259**, 220 (1999), quant-ph/9905020.
[5] P. Dorey, C. Dunning and R. Tateo, J. Phys. A **34**, (2001), 5679-5704, hep-th/0103051.
[6] A. Mostafazadeh, J. Math. Phys. **43**, (2002), 205-214, math-ph/0107001.
[7] C. M. Bender, Repts. Prog. Phys. **70**, (2007), 947-1018, hep-th/0703096.
[8] S. Weigert, Czech. J. Phys. **54**, (2004), 1139-1142, quant-ph/0407132.
[9] For an overview see, e.g., the special issues [76–78].
[10] T. Kato, *Perturbation theory for linear operators* (Springer, Berlin, 1966).
[11] H. Baumgärtel, *Analytic perturbation theory for matrices and operators*, (Akademie-Verlag, Berlin, 1984, and Operator Theory: Adv. Appl. **15**, Birkhäuser , Basel, 1985).
[12] N. Moiseyev and S. Friedland, Phys. Rev. A **22**, (1980), 618 - 624.
[13] W. D. Heiss and W. H. Steeb, J. Math. Phys. **32**, 3003 (1991).
[14] A. Mondragón and E. Hernández, J. Phys. A: Math. Gen. **26**, 5595 (1993).
[15] C. Dembowski *et al* , Phys. Rev. Lett. **86**, (2001), 787.
[16] P. Dorey, C. Dunning and R. Tateo, J. Phys. A **34**, L391 (2001), hep-th/0104119.
[17] M. V. Berry and M. R. Dennis, Proc. R. Soc. A **459**, 1261 (2003).
[18] E. Narevicius, P. Serra and N. Moiseyev, Europhys. Lett. **62**, 789 (2003).
[19] F. Keck, H. J. Korsch and S. Mossmann, J. Phys. A: Math. Gen. **36** (2003) 2125-2137.
[20] O. N. Kirillov and A. P. Seyranian, SIAM J. Appl. Math. **64**, (2004) 1383.
[21] M. V. Berry, Proc. R. Soc. A **461**, (2005), 2071.
[22] A. P. Seyranian, O. N. Kirillov and A. A. Mailybaev, J. Phys. A **38**, (2005), 1723, math-ph/0411024.
[23] U. Günther and F. Stefani, Czech. J. Phys. **55** (2005) 1099, math-ph/0506021.
[24] M. Znojil, Phys. Lett. B **650** (2007) 440, quant-ph/0701232.
[25] U. Günther, I. Rotter and B. Samsonov, J. Phys. A **40**, (2007), 8815-8833, math-ph/0704.1291.
[26] E. Caliceti, S. Graffi and J. Sjoestrand, J. Phys. A **40**, (2007), 10155-10170, math-ph/0705.4218.
[27] P. Cejnar, S. Heinze and M. Macek, Phys. Rev. Lett. **99** (2007) 100601, quant-ph/0707.2473.
[28] B. Bagchi, C. Quesne and R. Roychoudhury, J. Phys. A **41**, (2008), 022001, quant-ph/0710.1802.
[29] S. Weigert, J. Phys. A **39**, (2006), 10239-10246, quant-ph/0602141.
[30] M. Greiner, O. Mandel, T. Esslinger, T.W. Hänsch, and I. Bloch, Nature **415**, (2002), 39.
[31] R. Franzosi and V. Penna, Phys. Rev. A **63** (2001) 043609, cond-mat/0006446.
[32] G. J. Milburn, J. Corney, E. M. Wright, and D. F. Walls, Phys. Rev. A **55** (1997) 4318.
[33] J. R. Anglin and A. Vardi, Phys. Rev. A **64** (2001) 013605, physics/0105072.
[34] M. Holthaus and S. Stenholm, Eur. Phys. J. B **20** (2001) 451.

[35] K. W. Mahmud, H. Perry, and W. P. Reinhardt, Phys. Rev. A **71** (2005) 023615, cond-mat/0312016.
[36] Biao Wu and Jie Liu, Phys. Rev. Lett. **96** (2006) 020405, cond-mat/0508008.
[37] M. Hiller, T. Kottos, and A. Ossipov, Phys. Rev. A **73**, (2006), 062625, cond-mat/0602626.
[38] I. Bloch, T. W. Hänsch, and T. Esslinger, Phys. Rev. Lett. **82**, (1998), 3008, cond-mat/9812258.
[39] F. R. Gantmacher, *The theory of matrices. Vol. 1*, (Providence, RI: AMS Chelsea Publishing, 1998).
[40] N. G. Chebotarev, *Newton's diagram and its role in the contemporary development of mathematics*, in: Collected papers on the tercentenary of Newton's birth, (Moscow, Acad. Sci. USSR, 1943), 99-126.
[41] M. M. Vainberg and V. A. Trenogin, *Theory of branching solutions of non-linear equations*, (Leyden, Noordhoff International Publishing, 1974).
[42] S. Inouye, M.R. Andrews, J. Stenger, H.-J. Miesner, D.M. Stamper-Kurn and W. Ketterle, Nature **392**, (1998), 151.
[43] J. Dixmier, *Enveloping algebras*, (North-Holland, Amsterdam, 1977).
[44] entry "Universal enveloping algebra" in Encyclopedia of Mathematics, Springer, http://eom.springer.de.
[45] P. Giorda, P. Zanardi, and S. Lloyd, Phys. Rev. A **68**, (2003), 062320, quant-ph/0308133.
[46] N. Ya. Vilenkin, *Special functions and the theory of group representations*, (Amer. Math. Soc., Providence, RI, 1968).
[47] A. Perelomov, *Generalized coherent states and their applications*, (Springer, Berlin, 1986).
[48] B. C. Hall, *Lie groups, Lie algebras, and their representations*, (Springer, New York, 2003).
[49] T. Ya. Azizov and I.S. Iokhvidov, *Linear operators in spaces with an indefinite metric* (Wiley-Interscience, New York, 1989).
[50] A. Dijksma and H. Langer, *Operator theory and ordinary differential operators*, in A. Böttcher (ed.) *et al.*, *Lectures on operator theory and its applications*, Providence, RI: Am. Math. Soc., Fields Institute Monographs, **Vol. 3**, 75 (1996).
[51] G. S. Japaridze, J. Phys. A **35**, 1709 (2002), quant-ph/0104077.
[52] U. Günther, F. Stefani and G. Gerbeth, Czech. J. Phys. **54**, (2004), 1075-1089, math-ph/0407015.
[53] H. Langer and C. Tretter, Czech. J. Phys. **54**, 1113 (2004).
[54] S. Albeverio and S. Kuzhel, Lett. Math. Phys. **67**, (2004), 223-238.
[55] U. Günther, F. Stefani and M. Znojil, J. Math. Phys. **46**, 063504 (2005), math-ph/0501069.
[56] T. Tanaka, J. Phys. A **39**, (2006), 14175-14203, hep-th/0605035.
[57] M. V. Berry and M. Wilkinson, Proc. R. Soc. Lond. **A392**, (1984), 15.
[58] entries "Semi-simple element" and "Semi-simple matrix" in online Encyclopaedia of Mathematics, Springer, http://eom.springer.de.
[59] A. P. Seyranian and A. A. Mailybaev, *Multiparameter stability theory with mechanical applications*, (World Scientific, Singapore, 2003).
[60] D. Trotman and L. C. Wilson (eds.), *Stratification, singularities and differential equations. Vol. II, Stratification and topology of singular spaces*, (Hermann, Paris, 1997).
[61] J. H. Wilkinson, *The Algebraic Eigenvalue Problem*, Oxford University Press, Oxford, 1965.
[62] Y. Ma and A. Edelman, Lin. Alg. Appl. **273**, (1998), 45-63.
[63] C. M. Bender, M. V. Berry and A. Mandilara, J. Phys. A **35** (2002), L467-L471.
[64] P. R. Subramanian and V. Devanathan, J. Phys. A **7**, (1974) 1995-2007.
[65] entry "Singular point" in online Encyclopaedia of Mathematics, Springer, http://eom.springer.de.
[66] A. Vardi and J. R. Anglin, Phys. Rev. Lett. **86** (2001) 568, physics/0007054.
[67] S. Mossmann and C. Jung, Phys. Rev. A **74** (2006) 033601, quant-ph/0604158.
[68] D. Witthaut, E. M. Graefe, and H. J. Korsch, Phys. Rev. A **73** (2006) 063609, quant-ph/0602163.
[69] E. M. Graefe, and H. J. Korsch, Phys. Rev. A **76** (2007) 03211, quant-ph/0611040.
[70] P. Schlagheck and T. Paul, Phys. Rev. A **73** (2006) 023619, cond-mat/0402089.
[71] E. M. Graefe and H. J. Korsch, Czech. J. Phys. **56** (2006) 1007.
[72] D. Witthaut, E. M. Graefe, S. Wimberger, and H. J. Korsch, Phys. Rev. A **75** (2006) 013617, cond-mat/0609683.
[73] R. Franzosi, R. Livi, and G.-L. Oppo, J. Phys. B **40** (2007) 1195.
[74] R. Livi, R. Franzosi, and G.-L. Oppo, Phys. Rev. Lett. **97** (2006) 060401.
[75] E. M. Graefe, H. J. Korsch, A. E. Niederle, F. Trimborn and D. Witthaut, in preparation.
[76] Czech. J. Phys **54**, (2004), 1005-1148, *Special issue devoted to the subject of PHHQP*.
[77] J. Phys. A **39**, (2006), 9963-10262, *Special issue dedicated to the physics of non-Hermitian operators*.
[78] Czech. J. Phys **56**, (2006), 885-1064, *Special issue devoted to the subject of PHHQP*.